Resistive reconnection

R. B. White

Plasma Physics Laboratory, Princeton University, Princeton, New Jersey 08540

The linear and nonlinear theory of resistive magnetohydrodynamic modes is reviewed, with particular emphasis on aspects figuring prominently in the behavior of magnetic confinement fusion devices.

CONTENTS

I. INTRODUCTION

One of the most important properties of an ideal magnetohydrodynamic plasma is the fact that the plasma is frozen to the magnetic flux lines. Thus most instabilities involve motion of field and plasma together, and the characteristic time scale for the motion is the Alfvén time τ_A. The magnetic surfaces form topologically distinct regions, with the total magnetic flux in a given region moving with the plasma. This topological constraint means that, in general, there may exist inaccessible states of lower magnetic energy near a given initial state. Magnetic reconnection consists in the growth of one or more regions, in terms of the total magnetic flux in the region, at the expense of other regions. It allows the plasma to slip through the magnetic field lines, makes these states accessible, and thus introduces a whole new class of instabilities to those treated by ideal magnetohydrodynamics (MHD). The physical mechanism responsible for the partial decoupling of plasma and magnetic field lines takes the form of noninfinite current conductivity σ, which is traditionally described in terms of the plasma resistivity $\eta = 1/\sigma$ occurring in Ohm's law. The rate at which the magnetic field lines diffuse through the plasma is proportional to the plasma resistivity, giving rise to a second time scale defined by τ_R. Simple resistive diffusion is generally much slower than the ideal plasma response defined by τ_A, but special field configurations can give rise to much more rapid diffusion. In these configurations, plasma is forced toward a null line, where some component of **B** changes sign. An x point forms, with the field oriented in the four regions as shown in Fig. 1. In a resistive layer in the vicinity of the x point the field lines are reconnected, following the plasma flow in along the x axis and out along the y axis, as shown by the thick arrows. The nature of the forces driving the flow depend

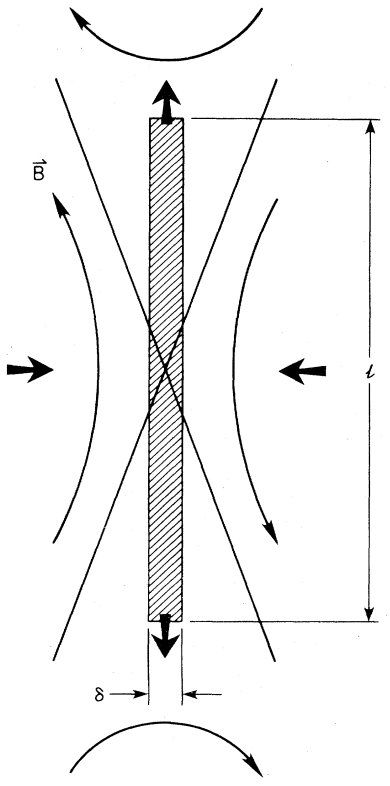

FIG. 1. The formation of an x point at a surface where one component of B changes sign. Reconnection occurs in the shaded area.

on global magnetic field configuration and boundary conditions. Thus the rate for the reconnection is a hybrid of the resistive rate τ_R^{-1} related to the diffusion and the rate at which the plasma and magnetic field are delivered to and from the x point, given by τ_A^{-1} when this occurs through ideal MHD processes. The reconnection time is given by $\tau = S^p \tau_A$, where $S = \tau_R / \tau_A$ is the Lundquist number and the power p depends on the self-consistent geometry and magnetic field determined by the boundary conditions and the nature of the driving forces, and varies from zero to one. In present-day fusion research devices $S \approx 10^7$, so the reconnection rate can vary greatly depending on the value of p.

The tearing mode, for example, consists of the growth of a magnetic island configuration. It occurs when the current profile causes an increase in island size to lead to a state of lower magnetic energy. When the perturbation is small, so that the island itself is smaller than the resistive layer, the driving forces produce reconnection with $p = \frac{3}{5}$. When the island grows to be larger than the resistive layer, nonlinear effects cause the growth to slow until $p = 1$. In toroidal geometry the value of p depends on the poloidal mode number m. Ideal driving forces can deliver magnetic flux to the resistive layer more rapidly for $m = 1$, giving $p = 0$ in the ideally unstable case, $p = \frac{1}{3}$ in the marginally unstable case, and $p = \frac{3}{5}$ in the stable case. For $m \neq 1$, $p = \frac{3}{5}$ for small islands and $p = 1$ when the island width exceeds the resistive layer width.

These cases, for which analytic solutions exist, illustrate the fundamental role of the global solution and boundary conditions in determining the reconnection rate.

Much of the history of a typical tokamak discharge is known, or conjectured, to be due to tearing-mode activity. In the initial stages of a discharge, the double tearing mode is thought to play a role in producing rapid current penetration into the plasma. During the discharge, there occur sawtooth oscillations and Mirnov oscillations, which are understood to be due to tearing modes, and the observed anomalous electron thermal transport is possibly due to small magnetic islands and resulting stochastic field behavior produced by microinstabilities. Finally, abrupt termination of a discharge, through what is referred to as a major disruption, is understood to be due primarily to tearing-mode activity. In addition, magnetic reconnection plays an important but perhaps less well-understood role in stellar and interstellar phenomena such as solar flares and the interaction of the solar wind with the Earth's magnetic field. This review will focus primarily on laboratory fusion-oriented plasmas, although much of the analysis is relevant also for astrophysical application.

In Sec. II we discuss magnetic surfaces. Section III describes the way in which plasma resistivity allows magnetic reconnection to occur. In Sec. IV the linear theory of the most important large-scale mode leading to magnetic reconnection, the tearing mode, is derived. How this mode is driven by the magnetic energy differential existing between the initial and final states is discussed in Sec. V. In Sec. VI these results are applied to cylindrical geometry, and the tearing mode is shown to be closely related to an ideal MHD mode, the kink mode. Finally, Sec. VII discusses the nonlinear theory of tearing-mode development and how this mode influences the evolution of a toroidally confined plasma.

The equations defining resistive magnetohydrodynamics are Ampere's law

$$\nabla \times \mathbf{B} = \mathbf{j} , \tag{1}$$

Faraday's law

$$\nabla \times \mathbf{E} = -\frac{\partial B}{\partial t} , \tag{2}$$

and Ohm's law

$$\mathbf{E} + \mathbf{u} \times \mathbf{B} = \eta \mathbf{j} . \tag{3}$$

Rationalized Gaussian units with $c = 1$ are used throughout. In addition are needed the equation of motion for the fluid, including $j \times B$, pressure gradient, and possibly viscous forces, and an equation of state to describe the pressure evolution in case plasma pressure plays a role.

II. MAGNETIC SURFACES

The existence of magnetic surfaces in magnetic confinement devices, or at least the existence of approximate magnetic surfaces over a large fraction of the plasma volume, is an essential requirement for long-term confinement. The existence of such surfaces has been shown only under fairly restrictive conditions (Morozov and Solov'ev, 1963). They are known to exist everywhere or in all but a small part of the plasma volume only when there exists a symmetry or approximate symmetry. This is easily demonstrated in cylindrical geometry for translational, axial, and helical symmetry. Writing the field in terms of the vector potential, $\mathbf{B} = \nabla \times \mathbf{A}$, the surfaces are defined by $A_z(r,\theta) = \text{const}$ in the case when A is translationally invariant in z, and $rA_\theta(r,z) = \text{const}$ in the case when A is independent of θ, and

$$A_z(r,\theta - az) + \alpha r A_\theta(r,\theta - \alpha z) = \text{const}$$

in the case when A is helically invariant; i.e., the magnetic surface depends only on the variables r and $\theta - \alpha z$. It is readily verified that these equations define surfaces to which B is tangent.

According to a theorem by Kolmogorov (1957), weak perturbation of a symmetric case leaves well-defined magnetic surfaces existing everywhere except in a small volume proportional to the square root of the perturbation, where the field assumes a stochastic character.

There is a close relation between the equations describing magnetic fields and Hamiltonian dynamics. Any magnetic field can be written

$$\mathbf{B} = \nabla \psi \times \nabla \theta + \nabla \varphi \times \nabla \psi_p(\psi,\theta,\varphi) , \tag{4}$$

with θ and φ arbitrary poloidal and toroidal angles (Boozer, 1983). The toroidal flux inside a constant ψ surface is $2\pi\psi$, and $2\pi\psi_p$ is the poloidal flux outside a constant ψ_p surface. The field lines are given by Hamilton's equations with φ the time variable and ψ_p the Hamiltonian,

$$\frac{d\psi}{d\varphi}=-\frac{d\psi_p}{d\theta}\ ,\quad \frac{d\theta}{d\varphi}=\frac{\partial\psi_p}{\partial\psi}\ . \tag{5}$$

Since

$$\mathbf{B}\cdot\nabla\psi=(\partial\psi_p/\partial\theta)(\nabla\varphi\times\nabla\theta)\cdot\nabla\psi\ ,$$

magnetic surfaces exist and are defined by ψ, provided ψ_p is independent of θ.

Surfaces are also known to exist in the vicinity of a closed field line (a fixed point of the mapping defined by the field) (Poincaré, 1892–1899). Consider a fixed-point trajectory given by $\psi_0(\varphi)$, $\theta_0(\varphi)$, with $\psi_0(2\pi)=\psi_0(0)$, $\theta_0(2\pi)=\theta_0(0)+2\pi m$. Consider trajectories near the fixed-point trajectory and expand the Hamiltonian equations about the fixed-point trajectory. Writing

$$\mathbf{V}(\varphi)=[\psi(\varphi)-\psi_0(\varphi),\theta(\varphi)-\theta_0(\varphi)]\ ,$$

we find a linear first-order differential equation for $\mathbf{V}$ with coefficients periodic in φ. Suppose two solutions to this equation, $\mathbf{V}_1(\varphi),\mathbf{V}_2(\varphi)$, have been found with the initial values $\mathbf{V}_1(0)=(1,0),\mathbf{V}_2(0)=(0,1)$. Then the solution for the initial condition $\mathbf{V}(0)=(a,b)$ is given by $\mathbf{V}=a\mathbf{V}_1(\varphi)+b\mathbf{V}_2(\varphi)$. Tracing a field line in successive passes in φ is thus reduced to a finite-difference equation for the coordinates (x_n,y_n) of $\mathbf{V}$ after n passes,

$$\begin{bmatrix}x_{n+1}\\ y_{n+1}\end{bmatrix}=(a_{ij})\begin{bmatrix}x_n\\ y_n\end{bmatrix}\ , \tag{6}$$

with $a_{ij}=[\mathbf{V}_1(2\pi),\mathbf{V}_2(2\pi)]$. From $\nabla\cdot\mathbf{B}=0$, it follows that $\det(a_{ij})=1$. If we attempt a solution of the form $x_n=C_1\lambda^n, y_n=C_2\lambda^n$, we find by substitution the characteristic equation

$$\lambda^2+(a_{11}+a_{22})\lambda+1=0\ ,$$

with a general solution of Eq. (6) given in terms of the two roots by

$$x_n=a_1\lambda_1^n+a_2\lambda_2^n\ ,\quad y_n=b_1\lambda_1^n+b_2\lambda_2^n\ . \tag{7}$$

The form of the trajectory depends on the magnitude of the trace of a_{ij}. If $|\alpha_{11}+\alpha_{22}|<2$, let

$$\cos\mu=(\alpha_{11}+\alpha_{22})/2\ ,$$

and the characteristics become $\lambda_{1,2}=\exp(\pm i\mu)$. A typical trajectory is given by

$$x_n=a\cos(\mu n)\ ,\quad y_n=b\sin(\mu n)\ , \tag{8}$$

and the fixed point is referred to as elliptical. The surface mapped out by Eq. (8) either forms a discrete set of points or is dense on the ellipse, depending on whether μ is a rational multiple of π.

If $|\alpha_{11}+\alpha_{22}|>2$, let

$$\cosh\mu=(\alpha_{11}+\alpha_2)/2\ ,$$

and the characteristics become $\lambda_{1,2}=\exp(\pm\mu)$. A typical trajectory is then given by

$$x_n=a\cosh(\mu n)\ ,\quad y_n=b\sinh(\mu n)\ , \tag{9}$$

and the fixed point is referred to as hyperbolic. In either case the surfaces are well defined. The approximation of linearizing the equations in the vicinity of the fixed point assumes that the sum over higher harmonics will not destroy the surfaces found. This has been shown by Arnol'd (1963) and Moser (1962). They proved that nonlinear terms lead only to a λ dependence of the coordinate, i.e., a distortion of the surfaces, but not to their destruction.

The first step in determining the degree to which such surfaces are destroyed is the determination of all instabilities that lead to magnetic reconnection. This was first carried out in a systematic manner by Furth, Killeen, and Rosenbluth (1963). Special cases had been considered earlier by various authors cited by them. Numerical confirmation of the analytically obtained growth rates was carried out by Wesson (1966).

Furth, Killeen, and Rosenbluth found three basic modes. The tearing mode is driven by magnetic free energy determined by the form of the current profile. It leads to the filamentation of the current and the formation of magnetic islands. Since the growth rate is largest for large-scale islands, this mode is the most important in describing global behavior in magnetic confinement fusion research devices. The second is the resistive g mode, driven by the expansion free energy associated with the pressure gradient and bad curvature. Finally, the rippling mode is driven by resistivity gradients. Both the resistive g mode and the rippling mode are most unstable for a small wavelength, and thus, although they may play some role in fine-scale plasma turbulence, do not contribute significantly to global plasma behavior. For this reason we shall concentrate our attention on the tearing mode.

III. PLASMA FIELD COUPLING

In ideal MHD [Eqs. (1)–(3) with $\eta=0$] the magnetic field lines are fixed in the fluid flow. Combining Eqs. (2) and (3) we find $\partial\mathbf{B}/\partial t=\nabla\times(\mathbf{u}\times\mathbf{B})$. Consider a surface and integrate this equation over it, giving

$$\partial\Phi/\partial t+\oint\mathbf{u}\cdot(d\mathbf{l}\times\mathbf{B})=0$$

with the flux $\Phi=\int d\mathbf{s}\cdot\mathbf{B}$, and $d\mathbf{l}$ an element of the surface boundary. This equation simply states that the flux convects with the fluid. Newcomb (1958) has shown rigorously that if two fluid elements are connected by a field line at one time, they remain so for all time.

The mechanism by which plasma remains attached to the field lines for small values of η is easily seen. Consider a field B_y and attempt to drive plasma across it by inducing a flow u_x. Then $\eta\mathbf{j}=\mathbf{u}\times\mathbf{B}$ gives $j_z=u_xB_y/\eta$, which induces a force $F=j\times B$ that has an x component

$F_x = -u_x B_y^2/\eta$ opposing the induced flow. This force is infinite in the limit $\eta \to 0$ provided $B_y \neq 0$. However, if B_y vanishes for some value of x, the opposing force also vanishes locally, and a field configuration can form about $x=0$ which gives rise to a rapid diffusion of the plasma through the field. Now suppose $B_y(x)=B_0$ for $x \gg L$, $-B_0$ for $x \ll L$, and vanishes along the surface $x=0$. Consider the magnetic flux passing through the xz plane, $\Phi(x)=\int^x B_y dx$. From Maxwell's equations and Ohm's law we find the local flux annihilation rate to be $\partial\Phi/\partial t = \eta\, \partial B_y/\partial x$, where we have ignored structure in the y direction, which we shall see is generally of larger scale than that in x. At $x=0$, depending on the nature of the driving forces, the field strength gradient $\partial B_y/\partial x$ can be made arbitrarily large, and thus an arbitrarily large reconnection rate can be attained for any finite η. A self-consistent solution shows that B_y is modified to produce a sharp gradient in a narrow range of x where the opposing force is small, $|x| < x_T$, referred to as the tearing layer. The width of this layer and the gradient of B_y depend on the nature of the driving forces. Rapid reconnection thus can occur only along surfaces defined by the vanishing of some component of B. In toroidal geometry these surfaces are those along which the toroidal and poloidal components of B describe a helix that completes an integer number of poloidal turns while completing an integer number of toroidal turns.

It is necessary to understand the nature of the driving forces in order to discuss meaningfully the reconnection rate. If the distant plasma is at rest, the reconnection is driven by the magnetic energy difference between the initial and final states, and the time scale for the mode growth is determined by a combination of the resistive and Alfvén times. Even so, the growth rate can be substantially different for different geometries. An inkling of this can be seen in the nonlinear behavior of certain ideal modes. The internal kink mode ($m=1$) nonlinearly evolves to a state with an infinite gradient of B across the singular surface. There is no similar phenomenon for $m \neq 1$. This tendency of the mode to develop a steep gradient in B leads to a much faster resistive growth rate in this case than for $m > 1$.

To discuss this more quantitatively, we represent the **B** field through the flux function $\psi(x,y)$ with

$$\mathbf{B} = \nabla\psi \times \hat{z} \tag{10}$$

and assume steady-state geometry given by Fig. 1. At large x an incompressible plasma is driven toward the x point with velocity **u**, imbedded in a field $\mathbf{B}=B_{y0}\hat{y}$. The configuration is symmetric in both x and y, with reconnection occurring in the neighborhood of the x point and the plasma flowing away in the y direction with velocity v and field $\mathbf{B}=B_{x0}\mathbf{x}$. Since the configuration is steady state, ψ has the form $\psi=\psi_0(x,y)-at$, and $\psi_0(x,y)$ has the shape of a saddle facing the y axis. The plasma pressure is $B_{y0}^2/2$ larger in the reconnection region than for $|x| > \delta$. This is balanced by the acceleration of the plasma along the y axis, up to kinetic energy $1/2\rho U_y^2 = B_{y0}^2/2$, giving $U_y \approx V_A$, the Alfvén speed. Equations (2) and (3) give

$$\frac{\partial\psi}{\partial t} + (U\cdot\nabla)\psi = \eta\nabla^2\psi + E\ . \tag{11}$$

Outside the reconnection region the rate of change of ψ is given by convection. Along the x and y axes this gives

$$\frac{\partial\psi}{\partial t} = U_{x0}B_{y0} = -V_A B_{x0}\ . \tag{12}$$

Mass conservation gives $U_{x0}l = V_A\delta$ and thus $B_{x0}=\delta/lB_{y0}$. At the x point, where there is no flow, $\partial\psi/\partial t$ is given entirely by $\eta j = \eta\nabla^2\psi \approx 2\eta B_{y0}/\delta$, and the width of the resistive layer δ must adjust until this value equals that determined by the boundary conditions. A dimensionless reconnection rate is defined as $M=(\partial\psi/\partial t)B_{y0}V_A$, and thus $M=2\eta/V_A\delta=\delta/l$ or $M=(\eta/V_A l)^{1/2}$.

There are two major models for steady-state reconnection, having to do with the size of the reconnection region, and in particular depending on the scaling of l with η. Writing $l=L/S^r$, where L is a fixed global length, we find $M\tau_A \sim S^{(r-1)/2}$. Sweet (1958) and Parker (1963) assumed that l had global dimensions ($r=0$), giving $M\tau_A \sim S^{-1/2}$. The current in the resistive layer, $j = V_A BM/\eta \sim S^{1/2}$, is singular in the limit $\eta \to 0$. The model proposed by Petschek (1964) attaches shock fronts to the diffusion region, which is similar to that in the Sweet-Parker model, but the length of the diffusion layer l is proportional to S^{-1} ($r=1$), giving M independent of η. The current is more singular than in the Sweet-Parker model, going as S for $\eta \to 0$. The introduction of the shocks, giving a more rapid reconnection rate, was proposed for the description of solar flares and the release of energy in the Earth's magnetosphere. For a review of these models see Vasyliunas (1975), Sonnerup (1979), and Hameiri (1979).

However, these analytical treatments leave many questions unanswered. Aside from the problem of smoothly matching the exterior solution to the diffusive region, the accessibility and stability of the steady-state patterns are not addressed by the analysis. This problem has been examined through numerical simulation with initial value codes. Simulations have succeeded in finding steady-state structure of the Petschek type (Ugai and Tsuda, 1977; Sato and Hayashi, 1979). The flow velocities were limited only by the local Alfvén speed, and shocks formed which were identified as slow shocks, satisfying the Rankine-Hugoniot conditions. However, this type of reconnection was observed only for an anomalous resistivity of the form $\eta \sim (j-j_0)^\nu$, where j_0 is a threshold value and ν a parameter of order unity. All simulations employing a resistivity that was a function only of position led to Sweet-Parker-type reconnection, with l independent of S (Waddell, Carreras, Hicks, and Holmes, 1976; Brushlinskii, Zaborov, and Syrovatskii, 1980; Priest, 1983; Park, Monticello, and White, 1984; Biskamp, 1985). The numerical simulations show that the situation that develops for small η, in fact, does not have a smooth transition at

the end of the diffusion layer. A negative-current region develops, which slows the velocity considerably below V_A. The simulations show that as η decreases, l increases until it attains the global system size, and a Sweet-Parker-type reconnection scaling occurs.

These results have also been observed experimentally (Stenzel, Gekelman, and Wild, 1982). Detailed spatial and temporal measurements of the vector electric field and current density during magnetic reconnection experiments were made. It was found that the resistivity was spatially very inhomogeneous but did not simply maximize in regions of large current densities, as would be required to obtain a Petschek-type reconnection.

The behavior of the current at the singular layer, $j \sim S^{(r+1)/2}$ as $\eta \to 0$, reveals the nature of the forces driving the instability. In both the Sweet-Parker and the Petschek models the plasma is asymptotically driven toward the resistive layer, producing a singular j at this point. This is also the case for the internal kink mode (Park, Monticello, White, and Jardin, 1980) and the ballooning mode (Monticello *et al.*, 1981). Thus, we conclude that when forces exist, even in the absence of resistivity, driving the plasma toward the singular surface, j will be singular and the reconnection will proceed at a rate faster than that given by the resistive time. An example of nonsingular behavior is provided by the nonlinear tearing mode for $m > 1$, which is stable in the limit $\eta \to 0$. The absence of driving forces means that j is finite for $\eta \to 0$ ($r = -1$), reconnection proceeds at the resistive rate.

IV. THE TEARING MODE IN SLAB GEOMETRY

In this section the growth rate for a magnetic island in slab geometry (Furth, Killeen, and Rosenbluth, 1963) is derived. The zeroth-order field is fixed in time, and all perturbations are required to vanish far from the singular surface. We take the initial field to be of the form

$$B_{y0} = \bar{B} F(x) , \quad B_z \gg \bar{B} , \quad B_{x0} = 0 , \tag{13}$$

where $F(x) \approx x$ for $x \ll 1$ and $F(x)$ is odd with $F(x) \to 1$ for $x \gg 1$. The distance from the singular surface x is normalized to the width of the current sheet

$$L^{-1} = (1/\bar{B})(\partial B_y/\partial x) ,$$

and B_z is constant in space. The plasma is initially stationary, $u_0 = 0$. Now $\nabla \cdot \mathbf{B} = 0$ is used to introduce a flux function $\psi(x,y)$ with

$$\mathbf{B} = \nabla\psi \times \hat{z} + B_z \hat{z} . \tag{14}$$

The scalar function ψ satisfies $\mathbf{B} \cdot \nabla\psi = 0$, i.e., $\mathbf{B}$ is tangent to surfaces of constant ψ. Moreover, from Eq. (1),

$$\nabla^2 \psi = -j_z . \tag{15}$$

Faraday's law gives for ψ

$$\partial\psi/\partial t + (\mathbf{u} \cdot \nabla)\psi = \eta \nabla^2 \psi + E , \tag{16}$$

where E is any externally imposed constant field which will be taken equal to zero. For the velocity, the electron equation of motion is used:

$$\rho \, d\mathbf{u}/dt = \mathbf{j} \times \mathbf{B} - \nabla p , \tag{17}$$

where (d/dt) is the convective derivative,

$$(d/dt) = (\partial/\partial t) + \mathbf{u} \cdot \nabla ,$$

and this equation is operated on with $\hat{z} \cdot \nabla \times$, also using the incompressibility of the plasma in the xy plane (large B_z) to introduce the velocity stream function φ with $\mathbf{u} = \nabla\varphi \times \hat{z}$. This gives

$$\rho (d/dt) \nabla^2 \varphi = -\hat{z} \cdot [\nabla\psi \times \nabla(\nabla^2 \psi)] . \tag{18}$$

Thus two coupled second-order partial differential equations are left for the scalar potentials φ and ψ. The zeroth-order state is completely described by $\psi_0'(x) = -\bar{B} F(x)$ and $\varphi_0 = 0$. The initial current-density profile is given by $j_{z0} = -\psi_0''$.

Equations (16) and (18) are now linearized, introducing a perturbation that will "interact" with the singular surface at $x = 0$, producing a periodic pattern of x points, each one having a magnetic field topology similar to that shown in Fig. 1. We write

$$\begin{aligned} \psi(x,y) &= \psi_0(x) + \psi_1(x) \cos ky , \\ \varphi(x,y) &= (\gamma/k\bar{B}) \varphi_1(x) \sin ky , \end{aligned} \tag{19}$$

where $\psi_1(x), \varphi_1(x)$ are assumed to vary in time as $e^{\gamma t}$. In Fig. 2 is shown the resulting pattern of magnetic field surfaces, $\psi = \text{const}$, forming a chain of islands. The value of ψ on the separatrix is found easily at the x point $\psi_s = \psi_0(0) - \psi_1(0)$, and setting $\psi(x,y)$ equal to this value for $y = 0$ and expanding $\psi_0(x)$ in a Taylor series about $x = 0$ gives for the island width

$$W = 4(-\psi_1/\psi_0'')^{1/2} . \tag{20}$$

Substituting Eqs. (19) into (16) and (18) gives two coupled second-order ordinary differential equations for $\psi_1(x), \varphi_1(x)$:

$$\psi_1(x) - F(x)\varphi_1(x) = (1/\gamma\tau_R)[\psi_1''(x) - k^2 \psi_1(x)] , \tag{21}$$

$$-\gamma^2 \tau_A^2 [\varphi_1''(x) - k^2 \varphi_1(x)] = F(x)[\psi_1''(x) - k^2 \psi_1(x)] - F''(x)\psi_1(x) , \tag{22}$$

where the primes denote d/dx and $\tau_A = \rho^{1/2}/(k\bar{B})$, $\tau_R = L^2/\eta$ are the characteristic Alfvén and resistive times for the problem. A number of assumptions are made at this point concerning the solution of these equations, which must be verified *a posteriori*. It is assumed that the growth rate is intermediate between ideal magnetohydrodynamic and resistive, i.e., $(1/\tau_R) \ll \gamma \ll (1/\tau_A)$. Further, it is assumed that the resistivity is relevant only in a narrow layer $x_T \ll 1$ where reconnection or tearing takes place.

Let us examine first the exterior region, where resistivity is assumed to be negligible. Assuming that scale

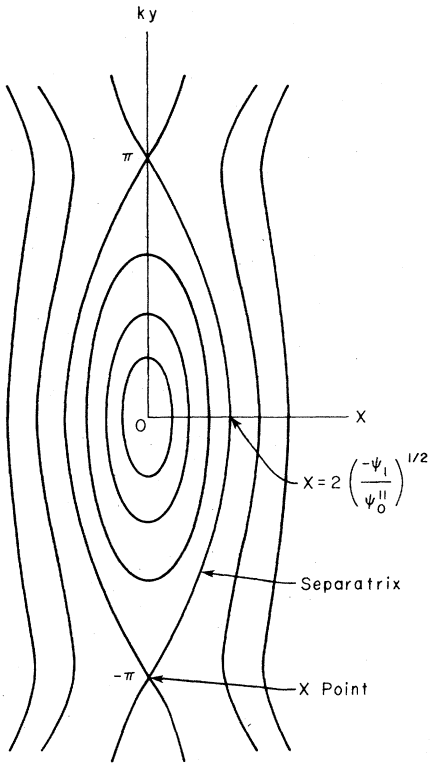

FIG. 2. A magnetic island. Shown are surfaces of constant ψ. The width of the island is the distance between separatrices perpendicular to the zeroth-order flux surfaces.

lengths for the solution are of the order of the shear length and using $\gamma\tau_A \ll 1$ gives

$$\psi_1(x)=\varphi_1(x)F\ ,\quad F(\psi_1''-k^2\psi_1)=F''\psi_1\ , \tag{23}$$

which for the particular profile $F(x)=\tanh x$ has the solution

$$\psi_1(x)=\exp(\mp kx)[1\pm(\tanh x)/k]\ , \tag{24}$$

where the upper (lower) sign corresponds to x positive (negative). The function $\psi_1(x)$ has a discontinuous derivative at $x=0$, and it is readily found that

$$\Delta'=\frac{\psi_1'(0+)-\psi_1'(0-)}{\psi_1(0)}=2\left[\left[\frac{1}{k}\right]-k\right]\ . \tag{25}$$

Note that Δ' is positive for $k<1$, i.e., when the shear length is short compared with the wavelength of the mode. Now the full resistive equations must be solved in the interior region and the solutions matched at the boundary. The fact that $x_T \ll 1$ is used, so that within the tearing layer $F(x)\approx x$. It is also assumed, from the nature of the exterior solution, that within the tearing layer $\psi_1(x)$ is approximately constant (the constant ψ approximation), although, of course, ψ_1' must be changing. Since $x_T \ll 1$, one can take $\psi_1'' \gg k^2\psi_1, \varphi_1'' \gg k^2\varphi_1$. Thus, Eqs. (21) and (22) give

$$\psi_1(0)-x\varphi_1=\psi_1''/\gamma\tau_R\ , \tag{26}$$

$$\gamma^2\tau_A^2\varphi_1''=-x\psi_1''\ , \tag{27}$$

and for the necessary matching to the exterior solution

$$-\frac{\gamma^2\tau_A^2}{\psi_1(0)}\int_{-\infty}^{\infty}\frac{\varphi_1''}{x}dx=\Delta'\ , \tag{28}$$

where an assumption has been made about the asymptotic behavior of φ_1 to extend the integral to $\pm\infty$, which will have to be checked *a posteriori*. The convergence of this integral guarantees that, asymptotically, the interior solution ψ_1 has constant slope and thus can be matched to the exterior solution. Introducing a new variable z through $x=(\gamma\tau_A^2/\tau_R)^{1/4}z$ and writing

$$\varphi_1=-(\tau_R/\gamma\tau_A^2)^{1/4}\psi_1(0)\chi(z)$$

gives

$$\chi''-z^2\chi=z\ , \tag{29}$$

which has the solution (Rutherford and Furth, 1971)

$$\chi=-\frac{z}{2}\int_0^1 du\,\exp(-\tfrac{1}{2}z^2\mu)(1-\mu^2)^{1/4}\ , \tag{30}$$

which can be verified by substitution. The solution is odd and also asymptotically equals $-(1/z)$. The matching condition becomes

$$\gamma^{5/4}\tau_R^{3/4}\tau_A^{1/2}\int_{-\infty}^{\infty}\frac{dz}{z}\chi''=\Delta'\ , \tag{31}$$

and $\gamma\tau_R\sim S^{2/5}\gg 1$ and $\gamma\tau_A\sim S^{-3/5}\ll 1$ as assumed. The integration in Eq. (31) can be truncated at $|z|=2$ with very little error. Thus, the tearing width will be arbitrarily set as $x_T=2(\gamma\tau_A^2/\tau_R)^{1/2}$, which is seen to scale as $S^{-2/5}$ times the shear length.

To evaluate the integral $I=\int_{-\infty}^{\infty}(dz/z)\chi''$, substitute Eq. (30) and integrate over z, giving

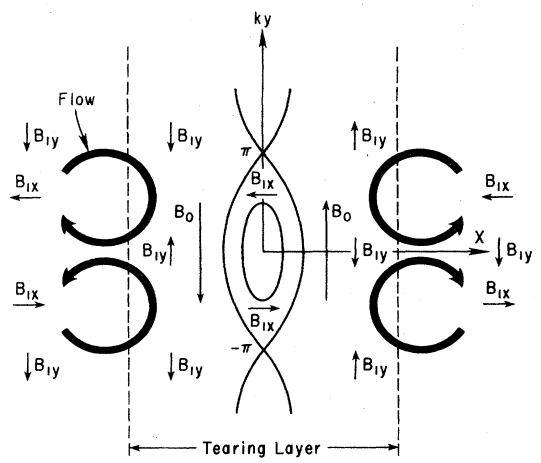

FIG. 3. The first-order fields and flow pattern associated with a linear tearing mode.

$$I=\left[\frac{\pi}{2}\right]^{1/2}\int_0^1 d\mu\frac{\mu^{1/2}}{(1-\mu^2)^{1/4}},$$

which is equal to $\pi\Gamma(\frac{3}{4})/\Gamma(\frac{1}{4})$. Thus,

$$\gamma=\left[\frac{\Gamma(\frac{1}{4})\Delta' L}{\pi\Gamma(\frac{3}{4})}\right]^{4/5}\tau_R^{-3/5}\tau_A^{-2/5}. \tag{32}$$

Note that long-wavelength modes are the most unstable. The physical origin of this effect is that the short-wavelength modes cause too much field line bending, which is stabilizing, compared to the gain in magnetic energy associated with island formation. Note that $\gamma\tau_R x_T=2\Delta' L^2$ and the tearing width is $x_T\approx 2(\Delta')^{1/5}S^{-2/5}$. In Fig. 3 are summarized the first-order fields and flow velocities.

V. MAGNETIC ENERGY OF THE TEARING MODE

In this section the magnetic energy available due to the formation of an island in slab geometry is calculated (Adler, Kulsrud, and White, 1980). The energy gained in island formation is proportional to Δ'. In addition to the net gain, there is a substantial energy transfer from the tearing layer outward.

The change in magnetic energy, $\frac{1}{2}\int |B|^2 dx\,dy$, in terms of the notation of the previous subsection, is given correctly to second order by

$$M=\tfrac{1}{4}\int dx[(\psi_1')^2+k^2\psi_1^2+4\psi_0'\psi_{20}'], \tag{33}$$

where

$$\psi(x,y)=\psi_0(x)+\psi_1(x)\cos ky+\psi_{20}(x)+\psi_{22}(x)\cos 2ky$$

and terms linear in $\psi_1(x)$ and $\psi_{22}(x)$ average to zero over y. Now one must find $\psi_{20}(x)$. Averaging the second-order part of Eq. (16) over y gives

$$2\psi_{20}(x)+\frac{1}{2}\frac{d}{dx}[\psi_1(x)\varphi_1(x)]=(\gamma\tau_R)^{-1}\frac{d^2\psi_{20}(x)}{dx^2}, \tag{34}$$

where $\eta=$const has been taken for simplicity. Terms proportional to $\nabla\eta$ can be shown to be negligible. The solution to Eq. (34) is

$$\psi_{20}=-\frac{1}{2\alpha}\int_{-\infty}^{\infty}dx'\exp(\alpha|x-x|)\frac{\partial}{\partial x'}K(x') \tag{35}$$

with

$$K(x')=\tfrac{1}{2}\gamma\tau_R\psi_1(x')\varphi_1(x'),\quad \alpha=(2\gamma\tau_R)^{1/2}.$$

The asymptotic form of Eq. (35) is readily evaluated, giving

$$\psi_{20}(x)\approx-\frac{1}{4}\frac{d}{dx}\left[\frac{\psi_1^2(x)}{F}\right]. \tag{36}$$

Unlike the exterior solutions for $\psi_1(x),\varphi_1(x)$, this expression is valid only for $x\gg(x_T/\Delta')^{1/2}$, i.e., the skin depth of the current sheet, and cannot be used in the vicinity of x_T.

To evaluate the change in the magnetic energy M, first consider the last term $M_3=\int_{-\infty}^{\infty}\psi_0\psi_{20}'dx$ and split it into two parts:

$$M_3=-\int_0^{\varepsilon}x\psi_{20}'dx+\tfrac{1}{2}\int_{\varepsilon}^{\infty}F\frac{d^2}{dx^2}\left[\frac{\psi_1^2}{F}\right], \tag{37}$$

where $(x_T/\Delta')^{1/2}\ll\varepsilon\ll 1$. Using $F(x)$ in the interior region and the asymptotic expression for $\psi_{20}(x)$ in the exterior region and integrating by parts, one finds for the total change in magnetic energy

$$M=\tfrac{1}{4}\int_{-\infty}^{\infty}dx[(\psi_1')^2+k^2\psi_1^2+(F''/F)\psi_1^2]+R. \tag{38}$$

Integrating the first term by parts, one finds that the integral in Eq. (38) is equal to $-(1/4)\Delta'\psi_1^2(0)$. Further, $|R|\ll\Delta'\psi_1^2(0)$ provided $\varepsilon>x_T^{1/3}/(\Delta')^{2/3}$, a reflection of the fact that the asymptotic form of ψ_{20} used for $x>\varepsilon$ is not valid for ε less than this value. Thus

$$M=-\Delta'\psi_1^2(0)/4. \tag{39}$$

The magnetic energy density can be directly evaluated in the interior region. Differentiating Eq. (35) gives

$$\frac{d\psi_{20}}{dx}=-\frac{1}{2\alpha}\int_{-\infty}^{\infty}dx'\exp(-\alpha|x-x'|)\frac{\partial^2}{\partial x'^2}K(x'), \tag{40}$$

which, upon integration by parts twice, gives

$$d\psi_{20}/dx\approx K(x) \tag{41}$$

plus terms of order αx, which are negligible provided $x<x_T$. One then finds for the magnetic energy density

$$\frac{\delta B^2}{2}=\frac{-\Delta'\psi_1(0)}{x_T}x\varphi_1(x), \tag{42}$$

which has a value of $-(\Delta'/x_T)\psi_1^2(0)$ at $x=x_T$. The total change in magnetic energy within $|x|<x_T$ is given by

$$M(x_T)=\frac{-\Delta'}{x_T}\psi_1(0)\int_{-x_T}^{x_T}x\varphi_1(x)dx. \tag{43}$$

Using Eq. (26) gives

$$M(x_T)=-\tfrac{3}{2}\Delta'\psi_1^2(0),$$

six times the entire change in magnetic energy. In Fig. 4 is shown schematically the change in magnetic energy density as a function of x, as found numerically using Eqs. (33) and (35). The surface terms in the integrations for $|x|<\varepsilon$ and $|x|>\varepsilon$ result from the energy transfer that takes place for $|x|>x_T$. Also shown is the divergent energy density obtained by using the exterior solution for ψ_{20} for $x<\varepsilon$.

Furth (1963) has derived a quadratic form that leads to a variational principle for the full resistive equations. He shows that this form gives a negligible contribution inside the tearing layer. In the exterior region this quadratic form is given by

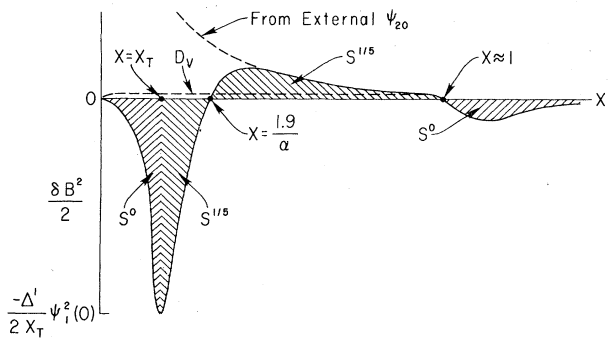

FIG. 4. The change in magnetic energy density produced by a magnetic island. Also shown is the divergent density obtained by using the asymptotic form of ψ_{20} for small x. The dotted line is the "energy" density obtained from a variational principle for the full resistive equations.

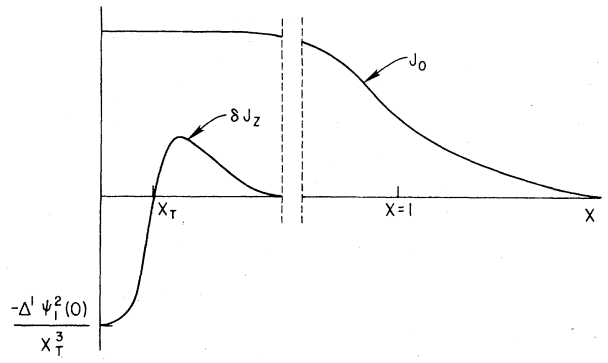

FIG. 5. The second-order eddy current, which produces the change in the magnetic energy for the mode and is responsible for the nonlinear algebraic growth.

$$V_0=\tfrac{1}{2}\int_\varepsilon^\infty dx\left[(\psi_1')^2+k^2\psi_1^2+\frac{F''}{F}\psi_1^2\right], \tag{44}$$

which is equal to M, from Eq. (38). The resulting "energy" density D_v is shown in Fig. 4. It is seen to agree with the magnetic energy density for large x and also has an integrated value of $-\Delta'\psi_1^2(0)/4$, although it is quite unlike the magnetic energy density for small x. The quadratic form V_0 is related to the infinite conductivity energy W_∞ (Bernstein, Frieman, Kruskal, and Kulsrud, 1958) by a singular term,

$$W_\infty=V_0+F'(\varepsilon)\psi_1^2(0)/2F(\varepsilon),$$

which is the result of integrating the last term in Eq. (44) by parts.

The total rate of change of energy inside a volume bounded by $a<x<b$ is due to the changes in magnetic and kinetic energy. These quantities have been evaluated (Adler, Kulsrud, and White, 1980) and shown to be equal to the work done by the pressure at the two boundary surfaces plus the energy radiated through the surfaces.

The kinetic energy $\frac{1}{2}\rho u^2$ is readily found from

$$\frac{d}{dt}K=\tfrac{1}{2}\gamma(\gamma^2\tau_A^2)\int_a^b[(\varphi_1')^2+k^2\varphi_1^2]dx\ . \tag{45}$$

The change in magnetic energy is given by Eq. (33):

$$\frac{d}{dt}M=\frac{\gamma}{2}\int_a^b[(\psi_1')^2+k^2\psi_1^2-4F\psi_{20}']dx\ . \tag{46}$$

There are two contributions to the energy balance at the surface, that due to the Poynting flux and that due to the work done by the pressure. To evaluate the Poynting flux, we use

$$P_x=(E_1\times B_1)_x+(E_2\times B_0)_x\ , \tag{47}$$

$$P_x=\gamma(-\psi_1\psi_1'\cos^2ky+2F\psi_{20})\ . \tag{48}$$

The work done by the pressure is given at each surface by pu_x, since the fluid is incompressible. To evaluate the pressure, we use $\nabla p=(j\times B)$, neglecting the density term in Eq. (14), which is of order $\gamma^2\tau_A^2$, to find

$$\frac{dp}{dx}=\frac{d}{dx}(F'\psi_1)\cos ky\ . \tag{49}$$

Evaluating these expressions using the explicit solutions in the interior and exterior domains, one finds energy conservation

$$\frac{d}{dt}\int_v(K+M)dx\,dy=-\int_S P\cdot dS-\int_S pu\cdot dS\ . \tag{50}$$

Shown in Fig. 5 is the second-order y-independent current density $j_z=-\psi_{20}''$. It arises physically through $u_1\times B_1$, and opposes j_{z0} inside the tearing layer and reinforces it outside. It is responsible for the change in the magnetic energy density by the induced change in B_y.

These results have been extended to include the case of an asymmetric current sheet by Bondeson and Sobel (1984). They found that there is an additional contribution to the magnetic energy, Eq. (39). The energy released takes the form

$$M=\tfrac{1}{4}\psi_1^2(0)[\Delta'+(\pi F''/F')^2/\Delta']$$

whether the plasma motion is inertial or viscous.

VI. CYLINDRICAL GEOMETRY

A. Introduction

In this section the equations used for the analysis of linear and nonlinear tearing-mode behavior in toroidal devices are developed. An examination of nonlinear behavior demands that one consider the interaction of the island both with the tearing layer itself and with the shear.

As originally pointed out by Shafranov (1970), the ideal magnetohydrodynamic kink instabilities are so strongly growing that the toroidal curvature has a very minor effect on the modes, and they can be analyzed to good ap-

proximation in cylindrical geometry. The same is true for the tearing mode, since its behavior is primarily governed by the magnetic energy driving it. It was shown by Furth, Rutherford, and Selberg (1973) that the toroidal curvature, for very small resistivity, does result in a small reduction of the tearing-mode growth rate. Glasser, Greene, and Johnson (1976) further showed that toroidicity improves the stability of the mode through the introduction of a threshold.

The effect of curvature, finite pressure, and magnetic interchange were considered by Kotschenreuther, Hazeltine, and Morrison (1985). Although modification of the threshold and growth rate in the linear regime were found, these effects were found to be progressively less important with increasing island width.

B. The reduced equations

As in Sec. II, we begin with Faraday's law, Ampere's law, the simplified form of Ohm's law, and the equation of motion. Tearing-mode behavior is governed primarily by the current profile, but can also be influenced by pressure, density, and resistivity profiles. When one or more of these is taken into account, equations that describe their evolution are also needed. Realistic treatment of the evolution of the resistivity profile requires the consideration of transport, ohmic heating, radiation, and impurities, and is beyond the scope of this review.

The geometry and notation for variables is shown in Fig. 6. Tokamaks are characterized by values of the safety factor $q(r)=rB_\varphi/(RB_\theta)$ of order unity and values of the inverse aspect ratio $\varepsilon=a/R_0$ much less than unity. The equations are thus expanded in the inverse aspect ratio, allowing the ratio of plasma pressure to magnetic field pressure $\beta=2p/B^2$ to be of order ε or smaller (Rosenbluth, Monticello, Strauss, and White, 1976; Strauss, 1976). Choosing B_φ and q to be of order unity leads to $B_\perp \sim O(\varepsilon)$. The divergence of the flow, $\nabla\cdot\mathbf{u}$, is found to be of order ε^3, which is important numerically since it eliminates the magnetosonic waves from the system, the fastest wave present being the incompressible Alfvén wave. The following consistent ordering scheme for resistive magnetohydrodynamic motion is found:

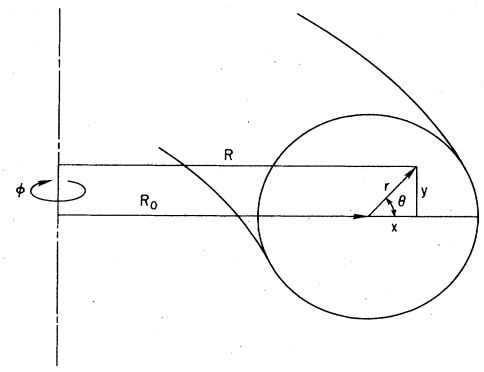

FIG. 6. Geometry for the description of a toroidal field.

$$
\begin{aligned}
&O(1):\ B_\varphi,\rho,\nabla_\perp\ ,\\
&O(\varepsilon):\ B_\perp,j_\varphi,u_\perp\frac{\partial}{\partial t},\frac{1}{R}\frac{\partial}{\partial\varphi}\ ,\\
&O(\varepsilon^2):\ \tilde{B}_\varphi,j_\perp,u_\varphi\ ,\\
&O(\varepsilon^3):\ \nabla_\perp\cdot u_\perp\ ,
\end{aligned}
\tag{51}
$$

and the pressure is taken to be either of order ε (high-beta three-dimensional equations) or of order ε^2 (low-beta three- or two-dimensional equations). Here

$$\nabla_\perp=\hat{r}(\partial/\partial r)+\hat{\theta}(1/r)(\partial/\partial\theta)\ ,$$

and more generally the subscript $\perp$ denotes perpendicularity to $\hat{\varphi}$. The equations have been extended to include terms up to fifth order by Izzo *et al.* (1985). These equations then include toroidal effects (Glasser, Greene, and Johnson, 1976) and plasma pressure for β of order ε or smaller. They also show that the fifth-order equations are the minimal reduced equations, in that they form the highest-order set that does not contain the fast magnetosonic waves.

Considerable success has been achieved by restricting consideration to following the nonlinear development of perturbations of a fixed helicity, thus reducing the number of dimensions of the problem from three to two (Rosenbluth, Monticello, Strauss, and White, 1976). In tokamaks the nonlinear coupling of modes of different helicities appears not to play an essential role except in final stages of development of large islands, which occur for particular current profiles. These phenomena, related to tokamak disruption, will be discussed in Sec. IV.

Fixed helical symmetry, together with cylindrical boundary conditions and equilibrium, implies that all quantities are functions of τ, r, and t only, where $\tau=m\theta+kz$ and $k=n/R_0$. Here m,n are the poloidal and toroidal mode numbers of the initial perturbation, which has the form

$$f(r)\exp[i(m\theta+kz)]\ ,$$

and the torus has been replaced by the equivalent cylinder with length $L=2\pi R_0$, and the φ coordinate with $z=R_0\varphi$. The helical symmetry allows the z coordinate to be eliminated through

$$\partial/\partial z=(k/m)(\partial/\partial\theta)\ .$$

In addition, this symmetry, together with $\nabla\cdot B=0$, implies that B can be written in terms of a scalar $\psi(r,\theta)$:

$$\mathbf{B}=\nabla\psi\times\hat{z}-(kr/m)B_z\hat{\theta}+B_z\hat{z} \tag{52}$$

and ψ is a flux function, i.e., $\mathbf{B}\cdot\nabla\psi=0$. In a cylindrically symmetric state, $\psi(r)$ is the flux through a helical ribbon defined by the magnetic axis and a helix of constant τ at minor radius r (Fig. 7). Vanishing of $(\partial\psi/\partial r)$ at $r=r_s$ means that the field through the helical ribbon vanishes at this point, and this condition determines a singular surface. In addition, ψ is related to the magnetic vector potential by $\psi=A_z-(kr/m)A_\theta$. The dynamical behavior of ψ follows from Faraday's law:

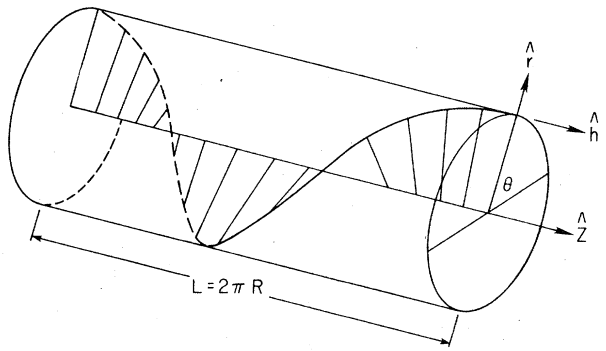

FIG. 7. The helical ribbon defined by the magnetic axis and a helix of constant $m\theta+kz$, r. At a singular surface the magnetic field vector is tangent to the ribbon.

$$\frac{\partial\psi}{\partial t}+\mathbf{u}\cdot\nabla\psi=-\eta j_z+E\ , \tag{53}$$

where E is an imposed electric field at the tokamak wall. The z component of the current is related to ψ through Ampere's law,

$$j_z=-\nabla^2\psi-2kB_z/m\ . \tag{54}$$

Note that for m,n positive we find at a rational surface ($\psi'=0$), from Eq. (52), that $B_\theta/B_z<0$, i.e., $j_z<0$ in this coordinate system. Incompressibility is again used to reduce the number of variables through the introduction of the potential φ with $\mathbf{u}=\nabla\varphi\times\hat{z}$.

Substituting Eq. (52) into the equation of motion and keeping only lowest order in ε gives

$$\rho\frac{d}{dt}u_\perp+\nabla_\perp\left[P+\frac{B^2}{2}-\frac{(\nabla_\perp\psi)^2}{2}+\frac{2kB_z\psi}{m}+\frac{1}{2}\left[\frac{kB_z r}{m}\right]\right]+\nabla_\perp\psi\nabla^2\psi=0\ , \tag{55}$$

which gives, upon operation with $\hat{z}\cdot\nabla\times$,

$$\frac{d}{dt}(\nabla_\perp\cdot\rho\nabla_\perp\varphi)=-\hat{z}\cdot[\nabla_\perp\psi\times\nabla_\perp(\nabla_\perp^2\psi)]\ . \tag{56}$$

These equations have been used in numerical codes to investigate the nonlinear development of modes with $m\geq 2$ (Danilov, Dnestrovskii, Kostomarov, and Popin, 1976; White, Monticello, and Rosenbluth, 1977; Biskamp and Welter, 1978; Waddell, Jahns, Callen, and Hicks, 1978; Monticello, White, and Rosenbluth, 1979) and $m=1$ (Sykes and Wesson, 1976; Waddell, Rosenbluth, Monticello, and White, 1976; Dnestrovskii, Lysenko, and Smith, 1977) and to construct analytic models for the nonlinear behavior of modes with $m\geq 2$ (White, Monticello, Rosenbluth, and Waddell, 1977a).

C. The tearing mode

Evolution of a mode is generally followed by perturbing a θ-independent equilibrium, specified by $j(r)$ or, equivalently, $q(r)$. From the definition of the safety factor we have

$$q(r)=\frac{r}{R[\psi'(r)+(kr/m)]}\ . \tag{57}$$

Using Eq. (32) and expressing the result in terms of the characteristic Alfvén and resistive times for the torus

$$\tau_A=(\rho^{1/2}am/B_z)=(\rho^{1/2}a^2m/\bar{B}R)\ ,\quad \tau_R=a^2/\eta\ ,$$

and using $k=n/R, F'=L^{-1}=\psi_0''$ gives

$$\gamma=[m\psi_0''(r_s)]^{2/5}(\Delta' a)^{4/5}\tau_R^{3/5}\tau_A^{-2/5}\ . \tag{58}$$

To determine Δ' and the radial dependence of other quantities in the linear theory, we linearize Eqs. (53) and (56) through

$$\begin{aligned}\psi&=\psi_0+\psi_1\cos m\theta\ ,\\ \rho&=\rho_0+\rho_1\cos m\theta\ ,\\ \varphi&=\varphi_1\sin m\theta\ ,\\ j&=j_0+j_1\cos m\theta\ ,\end{aligned} \tag{59}$$

where all first-order quantities are assumed to vary as $e^{\gamma t}$; we then eliminate all but ψ_1,φ_1, obtaining

$$\gamma\nabla\cdot\rho_0\nabla\varphi_1=\left[\frac{m}{r}\right](\psi_0'\nabla_m^2\psi_m-m\psi_1\psi_0'')\ , \tag{60}$$

$$\gamma\psi_1+\left[\frac{m}{r}\right]\psi_0'\varphi_1=\eta\nabla_m^2\psi_1 \tag{61}$$

with

$$\nabla_m^2=(1/r)(\partial/\partial r)r(\partial/\partial r)-m^2/r^2\ .$$

Assuming, as in Sec. IV, that $\gamma\tau_A\ll 1$, we find that, away from the singular surface,

$$\nabla_m^2\psi=-\frac{dj_0}{dr}\frac{\psi_1}{\psi_0'}\ . \tag{62}$$

The stability of a cylindrical plasma to tearing modes is completely determined by the quantity Δ', which, as shown in Sec. III, describes the available magnetic energy for the formation of an island. Shafranov (1970) calculated Δ' for a constant-current profile of finite extent, and Furth, Rutherford, and Selberg (1973) carried out a detailed investigation of the dependence of Δ' on the profile shape. The determination of Δ' was made by integration of Eq. (62) in the exterior region. They introduced profiles which they called peaked, rounded, and flat, with associated safety factors

$$q(r)=q(0)[1+(r/r_0)^{2p}]^{1/p}$$

and $p=1$, 2, and 4, respectively. From Eqs. (54) and (57) it was found that the current associated with a given q profile is

$$j=-\left[\frac{2}{Rq}\right]+\frac{rq'}{Rq^2}\ , \tag{63}$$

which reduces in this case to

$$j=j(0)/[1+(r_0)^{2p}]^{1+(1/p)} .$$

Note that in this coordinate system, j is negative. The parameter r_0 describes the width of the current channel. Equivalently, the two free parameters can be chosen to be q on axis and the location of the singular surface r_s. The peaked model is found to be unstable to $m=2$ and 3 tearing modes. The rounded model is generally more unstable, the $m=2,3$ modes existing over a wider range of r_s and the $m=4$ mode also becoming unstable. The flat profile is even more unstable. The behavior of Δ' as $r_s\to 0$ is $\Delta'\to f(m)/r_s$. Glasser, Furth, and Rutherford (1977) investigated the optimization of stability for different current profile shapes and showed that it is possible to achieve simultaneous stability against all modes. For a review of stability boundaries for different m values and various profiles, see Wesson (1978).

D. The resistive kink mode

The free-boundary kink and the tearing mode can be viewed as two different limits of the same instability. In the case of the ideal kink the magnetic island must be located outside the plasma in the surrounding vacuum region, and is felt only as a distortion of the plasma-vacuum boundary. If a resistive plasma is introduced into the vacuum region, the magnetic reconnection is resistively limited and the growth rate of the mode accordingly modified. A simple derivation of the linear growth rate for the resistive kink mode is presented here, which makes obvious this close connection (Pogutse and Yurchenko, 1977).

Consider an equilibrium with a dense plasma and a constant current density extending to $r=r_1$, and a much less dense, resistive plasma, and zero current, for $r>r_1$. The safety factor is then constant for $r<r_1$ and parabolic for $r>r_1$. The singular surface is assumed to lie in the low-density resistive plasma. We begin with Eqs. (60) and (61). Away from the singular region ($r\approx r_s$) resistivity is unimportant, so $\nabla\psi\times\nabla j_z=0$, or $j_z=j(\psi)$. Linearizing this gives

$$j(\psi)=j_0(\psi_0)+\frac{dj_0}{dr}\frac{1}{\psi_0'}\psi_1\cos m\theta \tag{64}$$

and thus for a constant current equilibrium $j_1=0$, which along with Eq. (54) gives

$$\left[\frac{1}{r}\frac{\partial}{\partial r}r\frac{\partial}{\partial r}-\frac{m^2}{r^2}\right]\psi_1=0 . \tag{65}$$

Thus solving for $\psi_1(r)$ reduces to matching solutions of Laplace's equation in the three regions $r<r_1$, $r_1<r<r_s$, and $r_s<r<a$. To find the discontinuity in ψ_1' at $r=r_1$, one integrates Eq. (60) across the surface $r=r_1$, relating the discontinuity in φ_1' to that in ψ_1':

$$\rho_0\varphi_1'|_-^+=\frac{m}{\gamma r_1}(\psi_0'\psi_1'|_-^+ +\psi_1\psi_0''|_-^+) . \tag{66}$$

From Eq. (61), away from the singular surface, $\gamma\psi_1+(m\varphi_1 Q/R)=0$ with $Q=(1/q)-(n/m)$. Thus also

$$\gamma\psi_1'+m\varphi_1' Q/R=0 , \quad r<r_1 , \tag{67}$$

$$\gamma\psi_1'+m\varphi_1' Q/R+m\varphi_1 Q'/R=0 , \quad r>r_1 , \tag{68}$$

and $Q'=-2/(rq)$ everywhere outside the current column. The discontinuity at the singular surface is given by Δ'. Writing the solution to Eq. (60) as

$$\psi_1=\begin{cases}(r/r_1)^m , & r<r_1 ,\\ C_1(r/r_1)^m+C_2(r/r_1)^{-m} , & r_1<r<r_s ,\\ C_3(r/r_s)^m+C_4(r/r_s)^{-m} , & r_s<r<a ,\end{cases} \tag{69}$$

and choosing for simplicity $m/n-q(0)\ll m/n$, one finds that the matching conditions at $r=r_1$ give

$$C_2=(m-nq)^{-1}\left[1-\frac{\gamma^2(\tau_+^2-\tau_-^2)}{2Q}+\frac{\gamma^2\tau_-^2 n^2}{m^2Q^2}\right]\times\left[1+\frac{\gamma^2\tau_-^2 n^2}{m^2Q^2}\right]^{-1} , \tag{70}$$

where $\tau_\pm=\rho_\pm^{1/2}/(nB_z)$ are the characteristic Alfvén times of the inner and outer regions. Similarly from matching at $r=r_s$

$$\Delta'=\frac{(m/r_s)\{-h+hC_2[1-(r_1/r_s)^{2m}]-1+C_2[1+(r_1/r_s)^{2m}]\}}{1-C_2[1-(r_1/r_s)^{2m}]} , \tag{71}$$

where

$$h=[1+(r_1/a)^{2m}]/[1-(r_1/a)^{2m}] .$$

Equation (58), which also relates the quantity Δ' to the growth rate, together with Eqs. (70) and (71), now determines γ. The two limits are readily obtained. Letting $\Delta'=0$ and $\tau_-=0$,

$$\gamma^2\tau_+^2=\left[\frac{m}{nq}-1\right]^2\frac{2m^2}{(r_1/a)^{2m}-1}+\frac{2m^2}{nq}\left[\frac{m}{nq}-1\right] , \tag{72}$$

which is the growth rate of the kink mode. In this limit the island growth is impeded by the inertia of the central core rather than the resistive tearing. The tearing-mode limit is found by setting the density discontinuity equal to zero in Eq. (70), giving $C_2=(m-nq)^{-1}$, independent of γ, and resulting in the tearing mode growth rate. In Fig. 8 is shown the growth rate γ as a function of $S=\tau_R/\tau_A$. The close relation between these modes is intuitively useful, and it indicates that for fairly sharply limited current profiles and with rather large resistivity in the region out-

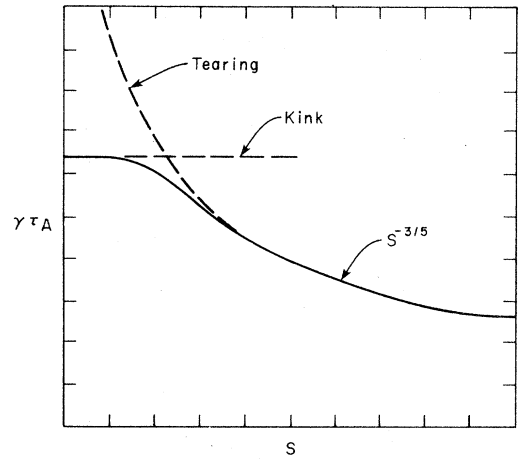

FIG. 8. Growth rate of the resistive kink modes as a function of S. Also shown are the tearing and kink mode growth rates.

side the current channel the nonlinear behavior of the tearing mode can be expected to be similar to that of the kink mode (Rosenbluth, Monticello, Strauss, and White, 1976).

E. The resistive internal kink mode

The internal kink mode, like the surface kink mode described in Sec. VI.D, has a resistive version. Recall that the ideal surface kink modes are unstable only when the singular surface $k\cdot B=0$ falls within the vacuum region.

Instability of the $m=1$ ideal internal kink mode does not depend on the singular surface lying within the vacuum. For finite resistivity the resulting mode can be expected to have quite different behavior, depending on whether the mode is ideally stable, neutral stable, or unstable. The linear growth rate can be calculated for the three cases in a single analysis (Coppi *et al.*, 1976).

We begin with the reduced equations of Sec. VI.B, valid to lowest order in kr/m, and perform the usual linearization, with

$$\psi=\psi_0(r)+\psi_1(r)\cos m\theta\ ,\quad \varphi=\varphi_1(r)\sin m\theta\ .$$

It is also convenient to express the equations in terms of the radial displacement

$$\xi(r)=[u_{1r}(r)/\gamma]=(m/\gamma r)\varphi_1(r)\ ,$$

and the radial magnetic field $b(r)=-(m/r)\psi_1(r)$, giving two coupled second-order differential equations:

$$\gamma b=m\gamma\xi\frac{\psi_0'}{r}+\eta\left[\frac{1}{r^3}\frac{d}{dr}r^3\frac{d}{dr}b-\frac{(m^2-1)}{r^2}\right] \tag{73}$$

and

$$\rho\gamma^2\left[\frac{1}{2}\frac{d}{dr}r^3\frac{d\xi}{dr}-(m^2-1)\xi\right]=-m\psi_0'\left[\frac{1}{r}\frac{d}{dr}r\frac{d}{dr}(rb)-\frac{m^2}{r^2}rb\right]+br\frac{d}{dr}\left[\frac{1}{r}\frac{d}{dr}(rm\psi_0')\right]\ , \tag{74}$$

where

$$\nabla^2(rf\cos m\theta)=[(1/r^2)(d/dr)r^3(d/dr)-(m^2-1)/r]\times f\cos m\theta$$

has been used. Recall that ψ_0' is simply related to the equilibrium safety factor through

$$\psi_0'=\frac{r}{R}\left[\frac{1}{q}-\frac{n}{m}\right]\ . \tag{75}$$

The standard method introduced in Sec. VI.C on the tearing mode is followed, i.e., it is assumed that the resistivity is negligible except in a layer surrounding $r=r_s$, the width of the layer to be determined in the course of the calculation.

First consider the exterior region. For zero resistivity, Eq. (73) gives

$$b=\left[\frac{m\psi_0'}{r}\right]\xi \tag{76}$$

which, upon substitution into Eq. (74), results in

$$\frac{d}{dr}\left\{r^3\left[\rho\gamma^2+\left[\frac{m\psi_0'}{r}\right]^2\right]\frac{d\xi}{dr}\right\}=g\xi\ , \tag{77}$$

with

$$g=[(m\psi_0')^2/r+\rho\gamma^2 r](m^2-1)\ .$$

Thus for $m=1$ the right-hand side of Eq. (77) vanishes, so a solution is $\psi(r)=$const. When we neglect $\rho\gamma^2$ with respect to $(m\psi_0'/r)^2$, the singular nature of the differential equation $[\psi_0'(r_s)=0]$ allows a continuity at the point $r=r_2$, and thus the solution to lowest order in kr/m consistent with the boundary condition $\psi(a)=0$ is

$$\xi_0(r)=\begin{cases}\xi_\infty\ , & r<r_s\ ,\\ 0\ , & r>r_s\ ,\end{cases} \tag{78}$$

valid in the exterior region ($\rho\gamma^2$ negligible).

Notice that the change in ξ (and ψ_1) of 100% across the inner region renders invalid the analysis of Sec. VI.C, based on the constant ψ approximation.

Now Eqs. (73) and (74) must be solved in the vicinity of the singular surface $r=r_s$ and the inner solution matched to the exterior solution. The matching turns out to be impossible to do with the lowest-order solution Eq. (78) because of the identical vanishing of g. It is necessary to find the exterior solution to the next order in the basic expansion parameter kr/m. One writes the solution to Eq. (77) as $\xi(r)=\xi_0(r)+\xi_1(r)+\cdots$, where the expansion pa-

rameter is kr/m. To obtain $\xi_1(r)$ one needs to find $g(r)$ to order $(kr/m)^2$. To do this, one returns to the equation of motion and linearizes, giving

$$\rho\frac{du}{dt}=-\nabla p_1+j_1\times B_0+j_0\times B_1 . \tag{79}$$

Now one applies $B\cdot\nabla\times$, giving on the right-hand side

$$\mathbf{B}\cdot\nabla(j_1\times B_0)+\mathbf{B}\cdot\nabla(j_0\times B_1) . \tag{80}$$

To all orders in kr/m

$$\begin{aligned} B_0&=\hat{z}B_z-\psi_0'\hat{\theta}-\left[\frac{kr}{m}\right]\hat{\theta} ,\\ \nabla&=\hat{r}\left[\frac{\partial}{\partial r}\right]+\hat{\theta}\left[\frac{1}{r}\right]\left[\frac{\partial}{\partial\theta}\right]+\hat{z}\left[\frac{\partial}{\partial z}\right] , \end{aligned} \tag{81}$$

and substituting $j_0=\nabla\times B_0$ and $j_1=\nabla\times B_1$ with $B_1=\nabla\psi_1\times\hat{z}$ gives, to order $(kr/m)^2$,

$$g=\left[\frac{(\psi_0'm)^2}{r}+\rho\gamma^2 r\right](m^2-1)+\left[\frac{kr}{m}\right]^2\frac{(\psi_0')^2}{r} . \tag{82}$$

The solution ψ_1 in the external region can now be found by integrating Eq. (77):

$$\frac{d\xi_1}{dr}=\begin{cases}\dfrac{\xi_\infty}{r(m\psi_0')^2}\displaystyle\int_0^r g\,dr, & r<r_s,\\ \dfrac{\xi_\infty}{r(m\psi_0')^2}\displaystyle\int_0^{r_s} g\,dr, & r>r_s,\end{cases} \tag{83}$$

from which it is apparent that

$$\frac{1}{\xi_\infty}\frac{d\xi_1}{dr}\to-\frac{\lambda_H}{\pi x^2} \tag{84}$$

near $r=r_s$, where $x=(r-r_s)/r_s$ and

$$\lambda_H=\frac{-\pi}{r_s[mr_sq'(r_s)/q]^2}\int_0^{r_s} g\,dr . \tag{85}$$

Here $\psi_0''=(-q'/q)(kr/m)$ at $r=r_s$ has been used. The quantity λ_H, having the dimensions of an inverse length, gives the effective width of the second-order exterior solution.

Now let us consider the interior region. In the vicinity of $x=0$, as long as $S=\tau_R/\tau_A\gg1$,

$$\begin{aligned}\frac{d^2\xi}{dx^2}&=\left[\frac{x}{\lambda^2}\right]\left[\frac{d^2\beta}{dx^2}\right] ,\\ \beta&=-\xi x+(S\lambda)^{-1}\left[\frac{d^2\beta}{dx^2}\right] ,\end{aligned} \tag{86}$$

where $\beta=b(r)(m\psi_0'')$, $\lambda=q\tau_H$, and τ_H^{-1} is the ideal free-boundary kink growth rate, $\tau_H=\rho^{1/2}/\psi_0''$. Now a solution of Eq. (86) is sought that can be smoothly joined to the exterior solution, Eq. (83). Combining the equations gives a fourth-order equation for ξ:

$$\frac{\lambda}{Sx}\xi''''-\frac{2\lambda}{Sx^2}\xi'''+\left[\frac{2\lambda}{Sx^3}-x-\frac{\lambda^2}{x}\right]\xi''-2\xi'=0 . \tag{87}$$

One solution is $\xi'=0$. The asymptotic behavior of the other three independent solutions for large $|x|$ are $\xi'\sim1/x^2$ and

$$\xi'\approx\exp[\pm x^2/(4\lambda/S)^{1/2}] .$$

From Eq. (84) the matching solution is a combination of the first ($\xi=$const) and second ($\xi'\approx1/x^2$). Note that asymptotic behavior of the other two solutions depends on η, and they therefore cannot be matched to the exterior solution. We write

$$\xi=\tfrac{1}{2}\xi_\infty+\xi_{\rm odd} \tag{88}$$

and impose the condition

$$\lim(x^2/2)(\xi_{\rm odd}'/\xi_{\rm odd})=-(\lambda_H/\pi)$$

for $x/\lambda\to-\infty$ as $\xi_{\rm odd}\to\xi_\infty/2$.

A numerical solution of Eq. (86) has been carried out using $\hat{x}=xS^{1/3}$. $\hat{\beta}=\beta S^{1/3}$, $\hat{\lambda}=\lambda S^{1/3}$. The results for $\xi_{\rm odd}$ are shown in Fig. 9 for various values of $\hat{\lambda}$. The boundary conditions imposed were that $\hat{\beta}(0)=1$ and $\xi_{\rm odd}(0)=0$, and $d\xi(0)/dx$ was adjusted until Eq. (85) was satisfied. In Fig. 10 is shown the growth rate as a function of the ideal magnetohydrodynamic growth rate measured by λ_H. Ideal marginal stability ($\lambda_H=0$) gives $\hat{\lambda}=1$ or $\lambda\sim S^{-1/3}$. If $\lambda_H\gg S^{-1/3}$, then $\lambda=\lambda_H$, i.e., the mode has the ideal growth rate. The growth rate is thus obtained in the following three cases: ideally unstable, $\gamma\sim(a/R)^2(1/\tau_H)$; ideally marginally stable, $\gamma\sim(a/R)^2S^{-1/3}(1/\tau_H)$; ideally stable, $\gamma\sim(a/R)^2S^{-3/5}(1/\tau_H)$.

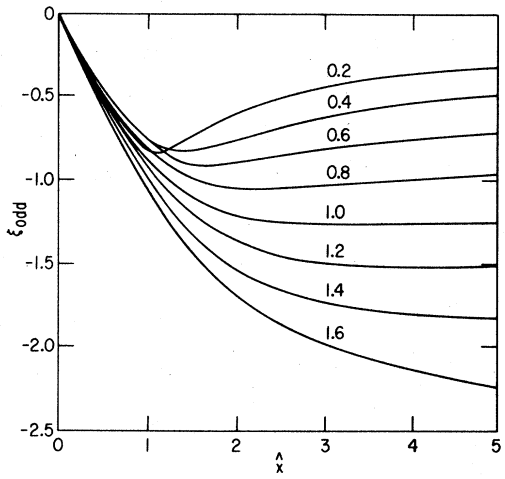

FIG. 9. Odd part, $-\frac{1}{2}\xi_\infty$, of the resistive layer solution ξ as a function of $\hat{x}=(r-r_0)/r_0S^{1/3}$ for different values of the normalized growth rate $\hat{\lambda}=\lambda S^{1/3}$. The eigenfunctions represented here have been derived by direct numerical integration. These agree with the analytical representation. Notice the change in the character of the eigensolutions as λ becomes smaller than unity, corresponding to $\lambda_H<0$.

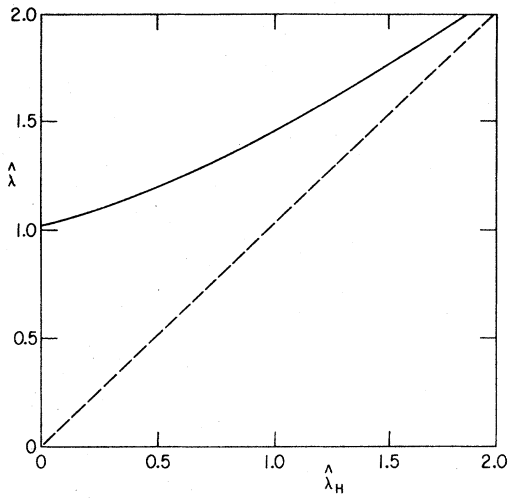

FIG. 10. The solid curve represents the growth rate as a function of the ideal MHD growth that is measured by $\hat{\lambda}_H=\lambda_H S^{1/3}$. This curve has been obtained by direct numerical integration.

Note that in the case of ideal stability the growth rate has the usual tearing-mode scaling found in Sec. IV. This scaling can be obtained, however, only if additional physical effects are present that can add stabilizing terms to $\int g(r)dr$. In cylindrical geometry the mode is always ideally unstable. In toroidal geometry the coupling of different m values produces a stabilizing effect, and the mode becomes unstable only for sufficiently large poloidal beta, typically $\beta_p>0.3$ (Bussac, Pellat, Edery, and Soule, 1977).

F. High β and multiple helicities

If the plasma pressure is taken to be of order ε, the equilibrium is θ dependent, modes of different helicities are coupled, and a full three-dimensional analysis is necessary. To find the equilibrium state, one writes the field in terms of the poloidal flux and the gradient operator in terms of the variables of Fig. 5,

$$B=\nabla A\times(\hat{\varphi}R_0/R)+B_\varphi\hat{\varphi}\ ,$$

with

$$\nabla=\hat{R}\left[\frac{d}{dR}\right]+\hat{\varphi}\left[\frac{1}{R}\right]\left[\frac{d}{d\varphi}\right]+\hat{y}\left[\frac{d}{dy}\right]\ .$$

One then finds

$$\nabla\times B=-\frac{\hat{\varphi}R_0}{R}\Delta^*A+\nabla(RB_\varphi)\times\frac{\hat{\varphi}}{R}\ , \tag{89}$$

where

$$\Delta^*=R\left[\frac{\partial}{\partial R}\right]\left[\frac{1}{R}\right]\left[\frac{\partial}{\partial R}\right]+\left[\frac{\partial^2}{\partial y^2}\right]\ .$$

Substituting this expression into $\nabla p=j\times B$ and using $p=p(A)$ gives

$$p'\nabla A=-(R_0^2/R^2)\Delta^*A\nabla A-RB_\varphi(1/R^2)\nabla(RB_\varphi)\ , \tag{90}$$

from which it can be concluded that RB_φ is also a function of A, in fact, equal to the total poloidal current. The equilibrium equation is thus found (Grad and Rubin, 1958; Shafranov, 1966):

$$-\Delta^*A=\frac{R^2}{R_0^2}p'(A)+\frac{II'(A)}{R_0^2}\ . \tag{91}$$

To lowest order in the inverse aspect ratio ε, the operator Δ^* reduces to $(\partial^2/\partial x^2)+(\partial^2/\partial y^2)=\nabla_\perp^2$, and the Grad-Shafranov equation becomes

$$\nabla_\perp^2A+\frac{2x}{R_0}\frac{\partial p}{\partial A}=\frac{II'(A)}{R_0^2}+p'(A)\ . \tag{92}$$

To lowest order in ε the expression for the magnetic field becomes

$$B=\nabla A\times\hat{\varphi}+B_\varphi\hat{\varphi} \tag{93}$$

and $j=\nabla\times B$,

$$j_\varphi=-\nabla_\perp^2A\ . \tag{94}$$

The incompressibility allows the velocity to be expressed as usual in terms of a scalar,

$$u=\nabla W\times\hat{\varphi}\ . \tag{95}$$

To complete the description of plasma evolution (Strauss, 1977), a closed set of coupled differential equations is found for the three scalars W, A, and p. The toroidal field $B_\varphi=I/R$, to lowest order, can be written as $B_\varphi=B_0+B_0R_0/R+I_1/R_0$, where the two corrections to the zeroth-order constant toroidal field are due, respectively, to toroidal curvature and plasma current. To lowest order in ε, $\nabla p=j\times B$ and thus

$$\nabla(p+B^2/2)=(B\cdot\nabla)B\ ,$$

which implies

$$\nabla(p+I^2/2R_0^2)=0\ . \tag{96}$$

Applying $\hat{\varphi}\cdot\nabla\times$ to the equation of motion then gives

$$\frac{d}{dt}(\nabla_\perp^2W)=\hat{\varphi}\cdot(\nabla A\times\nabla j_\varphi)+\frac{\partial}{\partial\varphi}\nabla_\perp^2A+2\left[\frac{\partial p}{\partial r}\sin\theta+\frac{1}{r}\frac{\partial p}{\partial\theta}\cos\theta\right]\ . \tag{97}$$

For the poloidal flux A, one begins with $\nabla_\perp\cdot B_\perp=0$, or $(\partial B_\perp/\partial t)=\nabla\times K$, which gives $(\partial A/\partial t)=K\cdot\varphi$. But from Ohm's law

$$\frac{\partial B_\perp}{\partial t}=\nabla\times\left[u_\perp\times B_\perp+\left[\frac{B_0}{R}\right]\left[\frac{\partial W}{\partial\varphi}\right]\hat{\varphi}-\eta j_\varphi\hat{\varphi}\right]\ ,$$

and thus

$$(\partial A/\partial t)=(B\cdot\nabla)W+\eta\nabla^2A$$

or

$$\frac{dA}{dt}=\frac{\partial W}{\partial \varphi}+\eta\nabla^2 A \ . \tag{98}$$

Finally, for the pressure,

$$dp/dt=0 \ . \tag{99}$$

These reduced equations have been used in three-dimensional numerical codes to investigate nonlinear tearing and ballooning modes (White, Park, Monticello, and Strauss, 1979; Strauss *et al.*, 1980) and in a low-β version (Biskamp and Welter, 1978; Dnestrovskii, Kostomarov, Pereverzev, and Tarasyan, 1978; Callen *et al.*, 1979; Dnestrovskii, 1979) to examine the nonlinear interaction of tearing modes of different helicities. Various numerical methods have been employed. The most successful uses Fourier decompositions in θ and φ, and a radial grid. Results obtained using these codes are discussed in the following sections.

VII. NONLINEAR THEORY

A. Introduction

Linear stability theory of the tearing mode gives only an incomplete description of the behavior of the mode, since in most laboratory plasmas nonlinear effects become important in the very early stages of development.

There are two separate nonlinear effects. The first, investigated by Rutherford (1973) and described in Sec. VII.B, occurs when the magnetic island width exceeds the width of the tearing layer. At this point, nonlinear currents dominate over the inertia, and the growth slows from exponential to algebraic, the island width increasing linearly in time. (The $m=1$ mode, in cylindrical geometry, is an exception to this because it is ideally neutral stable.) The second effect occurs when the island size becomes comparable with the shear length associated with the initial field. At this point, the behavior of the mode is dominated by the gross geometry, or equivalently by external driving forces. Magnetic energy is decreased within the island, but at the same time the curvature of the field lines outside the island increases the energy. The net change of energy for island growth depends on the island width and on the current profile. In cylindrical geometry with fixed boundary conditions, complete saturation of the mode can occur (White, Monticello, Rosenbluth, and Waddel, 1977a). The saturation is due to the existence of a geometry-dependent minimum magnetic energy state for a particular island width.

When the magnetic island is large compared with the tearing width, the plasma inertia becomes negligible, and the further evolution of the mode is governed by a nonlinear elliptic equation of state and an equation for the flux-line averaged time derivative of the magnetic flux. In this phase, development of the mode and response to variation of external boundary conditions results in adiabatic deformation of the state. Postulating that energy dissipation takes place only in a boundary layer near the separatrix, with the interior domains remaining classically adiabatic, allows the formulation of the problem in terms of jump conditions across the separatrices, similar to the Hygoniot conditions for an ideal shock (Grad, Hu, and Stevens, 1975).

B. Rutherford behavior

In this section the transition from exponential growth on a hybrid hydrodynamic-resistive time scale to algebraic growth on the resistive time scale (Rutherford, 1973) is reviewed. As shown in Sec. IV, there is a y-independent eddy current δj_z which opposes the zero-order current near the singular surface (see Fig. 5). This eddy current produces a third-order nonlinear force through $\delta j_z \times B_1$ which impedes the growth of the mode, and, since it is nonlinear, at some mode amplitude it replaces the inertia as the force opposing growth. To estimate the island width at which this will happen, consider Eq. (56):

$$\rho\frac{d}{dt}\nabla^2\varphi=-\hat{z}\cdot[\nabla\psi\times\nabla(\nabla^2\psi)] \ . \tag{100}$$

We shall consider the interior region for simplicity. Using the notation of Sec. IV we find

$$\gamma^2\tau_A^2\varphi_1''=-x\psi_1''-\psi_1\psi_{20}''/\bar{B} \ , \tag{101}$$

where the first term on the right-hand side is the linear driving force and the second is due to δj_z. Also from Sec. IV,

$$\psi_{20}'\sim K(x)=(\gamma/\eta\bar{B})\psi_1\varphi_1 \ . \tag{102}$$

Substituting this and making use of the constant ψ approximation, one finds that the nonlinear term will equal the left-hand side when $\gamma\tau_A^2=\psi_1/\eta\bar{B}^2$ or $w\approx x_T$. Furthermore, the sign of the nonlinear term is such as to replace the inertia term. In terms of Eq. (100), neglect of the inertia means that

$$\nabla\psi\times\nabla j=0 \tag{103}$$

or $j=j(\psi)$. The fluid velocity can also be eliminated from Eq. (53) for the magnetic flux by introducing the average along a flux line through

$$\langle F\rangle=\frac{\oint (dl/\nabla\psi)F}{\oint (dl/\nabla\psi)} \ .$$

Noting that $\langle u\cdot\nabla\psi\rangle=0$, one finds that the further evolution of the mode is governed by the two equations

$$\nabla^2\psi=-j(\psi) \ , \tag{104}$$

$$\langle\partial\psi/\partial t\rangle=-\langle\eta\rangle j(\psi)+E \ . \tag{105}$$

The approximate evolution of the mode in this regime is easily obtained. The island can be considered to be arbitrarily small (compared with the shear length), the linear approximations can be used for ψ,j. Substituting the expression for the mode, $\psi=\psi_0+\psi_1\cos ky$, and evaluating Eq. (105) at the 0 point, where the average over flux lines consists of the contribution from a single point, gives

$$\partial\psi_1(0)/\partial t = -\eta(0) j_1(0) \ . \tag{106}$$

Approximating j_1 as constant across the island and integrating Eq. (104) across the island by approximating $\nabla^2\psi_1\cos(ky)$ with $\psi_1''\cos(ky)$ gives

$$\partial\psi_1(0)/\partial t = \psi_1\Delta'/w\tau_R \tag{107}$$

or

$$(dw/dt) = \Delta'/\tau_R \ . \tag{108}$$

A more accurate integration of the flux surface averaged equations yields a factor of $\pi/2$ on the right-hand side of Eq. (108).

This analysis was extended to the collisionless ($\gamma \gg \nu$) and semicollisional ($\gamma \ll \nu$) regimes by Drake and Lee (1977). Modification of their results was carried out by Cowley, Kulsrud, and Hahm (1985). In these regimes the Doppler shift in the electron response prevents the complete shorting out of the field E_z by electron flux. It was found, however, that the collisionless and collisional modes evolve nonlinearly into the semicollisional regime, and that in this regime that mode again assumes the algebraic growth found by Rutherford (Monticello and White, 1980; Scott, Hassam, and Drake, 1985).

C. Nonlinear cylindrical modes, $m > 1$

1. Magnetic island saturation

Even algebraic growth, as discussed in Sec. VII.B, will typically produce a magnetic island that, barring some saturation mechanism, will fill the device in a time short compared with desired confinement times. The destructive properties of magnetic islands for confinement are apparent, magnetic surfaces providing rapid thermal conduction across the island and thus removing a large fraction of the insulating volume between the hot plasma center and the walls. There is, however, a natural saturation of the mode.

The saturation of the tearing mode occurs simply as the island grows, through the vanishing of the source of magnetic energy driving the instability. The saturation depends also on the form of the resistivity, but is rather insensitive to the exact form, provided the resistivity profile increases radially with approximately the scale length of the minor radius, as is normal. The fact that nonlinear coupling to other modes is not important in the saturation process makes a single helicity analysis possible. An analytical saturation model (White, Monticello, Rosenbluth, and Waddell, 1977a) is obtained as a quasilinear extension of the work of Rutherford described in Sec. VII.B. Beginning with the reduced equations for a mode of a single helicity derived in Sec. VI, and taking flux surface averages as in the last subsection, one obtains two equations that are the equivalent of Eq. (104) and (105) for cylindrical geometry,

$$\langle \partial\psi/\partial t \rangle = -\langle \eta \rangle j + E \ , \tag{109}$$

$$\nabla^2\psi = -j(\psi) - (2kB_z/m) \ . \tag{110}$$

For the flux topology of interest (a single island), the boundary conditions require the value of ψ at the 0 point as well as at the wall, or equivalently, the island width. The flux contours for an island in cylindrical geometry are shown in Fig. 11. It is readily verified that the perturbation expansion employed in Sec. IV,

$$\psi = \psi_0(0) + \varepsilon\psi_1(r)\cos m\theta + \varepsilon^2(\psi_2\cos 2m\theta + \delta\psi_0) + \cdots \ , \tag{111}$$

$$j = j_a(\psi_0 + \Delta\psi) + \varepsilon j^1(\psi_0 + \Delta\psi)\cdots \ , \tag{112}$$

is not applicable in the island interior. Here, $j_a(\psi_0)$ is the initial current profile. Note that $j_a(\psi)$ possesses many harmonics. It is evident from Fig. 12 that the separatrix is a highly singular point for the function $j(\psi)$. The harmonic expansion of ψ is, however, rapidly convergent for all r, even in the case of fairly large islands. We write

$$j(\psi) = \begin{cases} j_a(\psi), & \psi < \psi_s, \\ j_b(\psi), & \psi > \psi_s, \end{cases} \tag{113}$$

where ψ_s is the value of ψ on the separatrix, and model the current in the island interior through

$$j_b(\psi) = a + b\psi \ , \tag{114}$$

which can be regarded as a truncation of the Taylor expansion of $j(\psi)$. The form of the model was arrived at by examination of results of numerical advancement of the equations of Sec. VI. It was observed that saturation occurred with significant changes taking place only in the first and zeroth harmonic in the island vicinity. The coefficients in Eq. (114) can be determined by matching the interior and exterior regions, much as in Sec. IV, only now the interior refers to the island, not to the tearing layer. In terms of these harmonics Eq. (110) takes the form

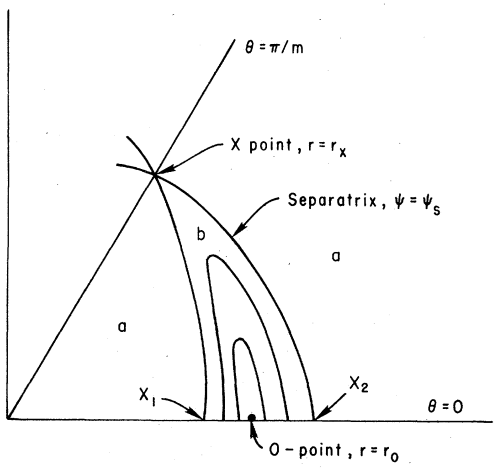

FIG. 11. Surfaces of constant $\psi(r,\theta)$ for a magnetic island. Region a, the exterior, and region b, the interior, are bounded by the separatrix $\psi = \psi_s$. The x point and 0 point are shifted outward and inward, respectively, from the resonant surface.

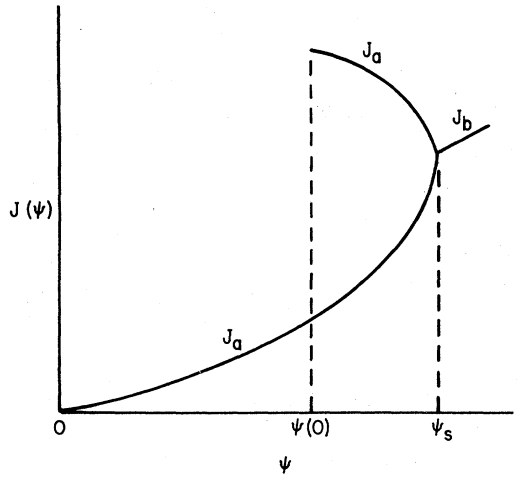

FIG. 12. The current profile $J(\psi)$ in the presence of an island. The subscripts refer to the regions of Fig. 11.

$$\delta\psi_0''=-(\delta\psi_0'/r)-\delta j_0\ ,$$
$$\psi_1''=(m^2/r^2)\psi_1-(1/r)\psi_1'-j_1\ , \tag{115}$$

where the harmonics of the current are given by

$$j_0(r)=(m/\pi)\int_0^{\pi/m}d\theta\, j(\psi)\ ,$$
$$j_1(r)=\left[\frac{2m}{\pi}\right]\int_0^{\pi/m}d\theta\, j(\psi)\cos m\theta\ , \tag{116}$$

and $\delta j_0=j_0(r)-j_a[\psi_0(r)]$.

Now we integrate Eq. (115) across the island and match to the exterior solution. This uniquely determines the state by determining the constants a,b in terms of the island width, which is a free parameter. This matching gives

$$a+b\psi_0(r_s)=j_0(r_s)$$

and $b\approx-\pi\Delta'(w)/w$ plus terms of higher order, which are negligible. Here $\Delta'(w)$ is the equivalent of Δ' in the linear theory,

$$\Delta'(w)=(\psi_{1+}'-\psi_{1-}')/\psi_1(r_s)\ ,$$

where $+,-$ refers to the island edges. Once this state is determined, Eq. (109) can be used to determine its growth rate. Subtracting the two values at the 0 and x points, we find

$$(dw/dt)=1.66\eta(r_s)[\Delta'(w)-\alpha w]\ , \tag{117}$$

where α depends on the resistivity profile, but is practically negligible if this profile is increasing radially with a scale length given by the minor radius. Note that the current inside the island is

$$j=j_0(r_s)-\pi[\Delta'(w)/w]\psi_1(r_s)\cos m\theta$$

and thus for a growing island the value of j at the 0 point

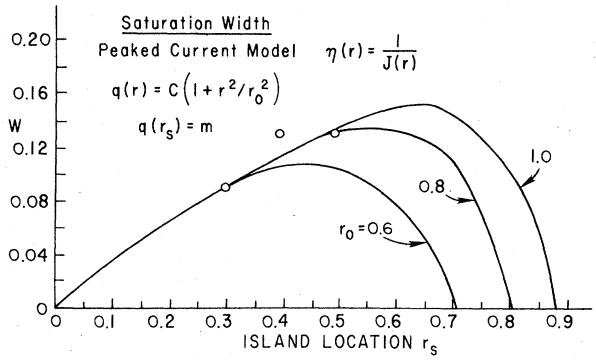

FIG. 13. Saturation width predicted using the quasilinear model for $m=2$. Here $J_a(r)$ is given by the peaked current model and the resistivity $\eta(r)\sim J_a(r)^{-1}$. The points are results of time-stepping the full nonlinear code for the case $r_0=0.8$.

is greater in magnitude than the value at the x point (recall $j<0$). In a saturated state the current density is approximately constant within the island. These results are confirmed in numerical simulations using the full resistive MHD equations.

In the absence of a temperature differential and current drive, the major role in Eq. (117) is played by the quantity $\Delta'(w)$, obtained from the exterior solution. For typical resistivity profiles the mode thus saturates approximately when $\Delta'(w)$ vanishes, and the saturated island width can be determined by a numerical evolution of $\Delta'(w)$. As was shown in Sec. VI, the most unstable modes were those with low values of m. The largest saturated island states also correspond to modes with $m=2$. The dependence of the saturation width on the island location, r_s, is shown in Fig. 13. This is to be contrasted with the dependence of Δ' on r_s, $\Delta'\to[f(m)]/r_s$ for small r_s. An example of the dependence on the saturation width on the form of the current profile is shown in Fig. 14 (Monticello, White,

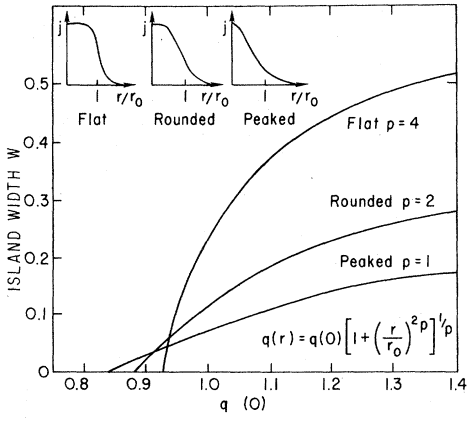

FIG. 14. Maximum island width as a function of the safety factor on axis $q(0)$ for a variety of current profiles. Only fairly flat profiles are capable of producing large islands. Here the $q=2$ surface is fixed at $r=0.7a$.

and Rosenbluth, 1979). Here, it is apparent that the flatness of the current profile, i.e., shear large only in the exterior region near the singular surface, is important for large-island development. In this figure the island position ($q=2$ surface) has been held fixed at $r_s=0.7a$ so that increasing $q(0)$, as well as increasing the parameter p, corresponds to flattening the profile. As long as the current profile is not too flat, the state of minimum energy consists of an island state with island width less than 10% of the minor radius. Inclusion of finite Larmor radius effects does not change the saturation width of this state, but causes a mode rotation at the diamagnetic frequency (Monticello, White, and Rosenbluth, 1979; Biskamp, 1979; Monticello and White, 1980; Scott, Hassam, and Drake, 1985). The resulting $m=2$ oscillations give a theoretical interpretation of the experimentally observed Mirnov oscillations (Mirnov and Semenov, 1971). These methods have been extended to toroidal geometry by Chu and Lee (1983) and Bateman and Morris (1985).

2. Island modification by local heating

Of some interest is the case where the island center has a temperature significantly different from the surrounding plasma, either through local heating or through radiative losses (Yoshioka, Kinoshita, and Kobayashi, 1984). In this case, using $\eta\sim T^{-3/2}$, the dominant contribution to α is

$$\alpha=-\frac{12}{\pi}\frac{j}{\psi_0''w^2}\frac{\delta T}{T}\ , \tag{118}$$

where δT is the temperature differential between the 0 point and the separatrix. The power balance for the temperature in the island is

$$-\int \kappa_\perp \nabla T\cdot ds=\int P\,dv\ , \tag{119}$$

where P is the net power deposited in the island (ohmic heating, radiation losses, etc.). For a thin island we have $\nabla T\approx -2\delta T/w$. Using the fact that the island volume-to-surface ratio is $dv/ds=w$ and $\psi_0''=-rq'B_T/Rq^2$, we find

$$\alpha=\frac{6}{\pi}\frac{Jq^2RP_v}{T\kappa_\perp rq'B_T}\ . \tag{120}$$

Thus excess radiative losses ($P_v<0$) destabilize the island, and localized heating has a stabilizing effect.

3. Island modification by current drive

Localized current drive can also modify the island development (Reiman, 1983). In the presence of current drive, Ohm's law is modified and Eq. (109) takes the form

$$\left\langle\frac{\partial\psi}{\partial t}\right\rangle=-\langle\eta(j-j_d)\rangle+E\ , \tag{121}$$

where j_d is an externally driven current. Evaluation of this expression at the x and 0 points gives, neglecting α,

$$\frac{d\psi_1}{dt}=\frac{\pi\eta\Delta'\psi_1}{w}+\eta(j_{d0}-j_{dx})\ . \tag{122}$$

Thus increasing the magnitude of the current at the 0 point is stabilizing (recall $j<0$).

4. Transport due to magnetic islands

Magnetic islands, by creating regions of enhanced transport, also modify the evolution of the current profile. Thus, by introducing models for the transport, a coupled system involving the current profile and magnetic islands is produced. The exponential growth phase of the islands occurs only when the island is so small as to be negligible. These models make use of the nonlinear saturation width of the island, obtained by setting $\Delta'(W)=0$. Several interesting qualitative features have been obtained by numerical simulation of tokamak discharges using models of this type (Wesson and Turner, 1982; Ivanov, Kakurin, and Chudnovskii, 1984). The occurrence of large islands is observed when the safety factor q at the plasma boundary approaches integer values. In the initial stages of a discharge, when the plasma current is increasing, magnetic islands are observed to develop to much larger size if the current is increased slowly than if it is raised quickly. This is simply due to the fact that Δ' remains favorable to large-island development for a very brief time during rapid current increase, and the islands do not have time to develop. In addition, fluctuations in the perturbation amplitude and the appearance of negative voltage spikes are observed. All of these phenomena are in qualitative agreement with experimental data. In addition, it has been proposed that small magnetic islands are responsible for the anomalous electron heat transport observed in tokamaks. The magnitude of this effect was examined by Boozer and White (1982) and White (1984) and the self-consistent effect of the islands on the current profile by Ivanov (1983).

5. Singular current sheets

As discussed in Sec. III, the behavior of the current at a surface where reconnection is occurring depends on the nature of the driving forces. Generally, a singularity occurs associated with a finite jump in magnetic field, i.e., $\int J\,dr$ across the reconnection layer in integrable and nonzero as $\eta\to 0$. In helical symmetry this jump in magnetic field can occur only on the resonant surface, but this constraint is relaxed in general three-dimensional plasma evolution. Current singularities can occur at unpredictable locations, as seen in ballooning mode simulations (Monticello *et al.*, 1981). These singularities then cause rapid reconnection, changing the magnetic topology on a time scale short compared to τ_R. In such a rapid relaxation process, the magnetic helicity will change slowly, since

$$d/dt\int A\cdot B\,d\tau\sim\int \eta J\cdot B\,d\tau\sim\eta\int J\,dr\sim\eta\ .$$

Thus magnetic helicity is conserved on the time scale of the topology change, as was assumed by Taylor (1974).

D. The major disruption

The major disruption occurring in tokamak discharges appears primarily to be due to a large $m=2$ magnetic island. There are a variety of guises in which the disruption can appear. At low plasma β, however, a canonical sequence is as follows: Some time is spent executing sawtooth oscillations (see Sec. VII.E), after which these oscillations cease and the so-called precursor oscillation, an $m=2$ mode, is observed to grow at a rate consistent with the Rutherford rate for a magnetic island. As shown by White, Monticello, and Rosenbluth (1977), a small change of a current profile associated with sawtooth oscillations [$q(0)\approx 1$] can lead from a case in which the $m=2$ mode is stable to one in which the saturation width is a large fraction of the minor radius. Furthermore, the growing island, by increasing radial transport, decreasing the current, and thus increasing the value of q, produces a profile unstable to even larger island growth, as seen in Fig. 14. This process, associated with the precursor oscillation, would, of course, result in the termination of the sawtooth oscillations with the elimination of the $q=1$ surface. The coupling of the precursor oscillation to other modes, particularly to $m=1$ through toroidal coupling, and the sensitivity of this coupling to the current profile (Bussac, Edery, Pellat, and Soule, 1977) provides for a wide variety of satellite modes in the predisruptive phase. The precursor oscillation is followed by the disruption itself—a rapid drop in central temperature and often a total loss of plasma. The disruption itself is thought to be caused by an onset of stochasticity induced by this $m=2$ island together with some combination of nonlinear coupling to other modes (Welter and Biskamp, 1978; Biskamp, 1978; Waddell, Carreras, Hicks, and Holmes, 1979; Callen *et al.*, 1979; Dnestrovskii *et al.*, 1979; Kleva, Drake, and Bondeson, 1984) toroidal coupling (Finn, 1975,1977; Kurita, Azumi, Tsunematsu, and Takeda, 1983), and contact with the limiter or walls (Pollard, Turner, Sykes, and Wesson, 1979; Sykes and Wesson, 1980). None of the proposed models gives a complete description of the final stages of the disruption. The mode coupling calculations, although giving rise to an explosive growth on a rapid time scale when the $m=2, n=1$ island overlaps an $m=3, n=2$ island, do not produce a rapid drop of central plasma temperature. The resulting stochastic region flattens the temperature between the $q=\frac{3}{2}$ and $q=2$ surfaces, but some further mechanism is required to destroy confinement in the central region. Significant mode coupling occurs for profiles that are unstable to fairly large $m=2$ island development, so the mode coupling model complements this description of the disruption rather than replacing it. The role of fine-scale fluid turbulence in the final stages of the disruption has been studied by Diamond *et al.* (1984), and

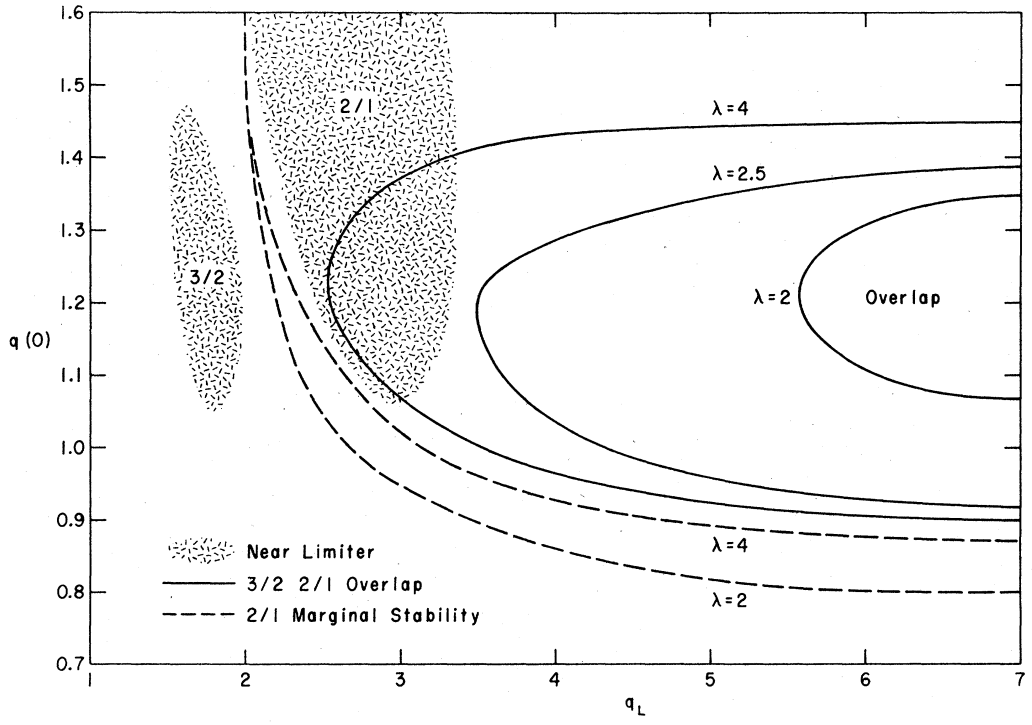

FIG. 15. Domains of island overlap. The profiles are those of Sec. III with $q(r)=q(0)[1+(r/r_0)^{2\lambda}]^{1/\lambda}$, and q_L is the value of q at the limiter.

preliminary results indicate a qualitative understanding of the time scales and magnitudes for the toroidal current diffusion and negative voltage spike. The role of limiter contact in the disruption is not yet certain. Model calculations including the interaction of an $m=2$ mode with the limiter do show plasma loss, but the time scale for this process with realistic plasma parameters is not known. Present experimental evidence makes it very plausible that there are many different forms of disruption, involving some combination of these, and perhaps yet other, processes. An interesting additional complication is the observation (Bondeson, 1983) that large $m/n=2/1$ island states can be ideally unstable to other helicities.

Current profile parameters for which an overlap of the $m/n=2/1$ and 3/2 islands occur, and for which limiter contact can occur, have been mapped out by White and Monticello (1980). These are shown in Fig. 15. The evolution of the islands in a case where strong overlap occurs has been carried out by Callen *et al.* (1979) and Carreras, Hicks, Holmes, and Waddell (1980). An example of island widths as a function of time is shown in Fig. 16. The profile used was that shown by White, Park, Monticello, and Strauss (1979) to give rise to a very large $m=2$ island, overlapping the $q=\frac{3}{2}$ surface. Note that the $m=2$ island actually further destabilized the $m=3, n=2$ island when they overlapped, producing violent nonlinear growth and stochastic fields.

Control of the disruption by feedback has been studied both experimentally (Arsenin and Chuyanov, 1977; Karger *et al.*, 1977; Arsenin, Arkmenkov, Ivanov, and Kakurin, 1978) and theoretically (Monticello, White, and Rosenbluth, 1979; Callen *et al.*, 1979).

Experimentally there appears to be a β limit to disruption-free tokamak discharges (Karger *et al.*, 1979), given approximately by

$$\beta_T \approx 3I/aB \tag{123}$$

with I in A, a in cm, and B in G. Numerically, it is found that such a limit is provided by the $n=1$ external kink mode (Troyon *et al.*, 1984). The highest β is reached when q on axis is slightly above one. This limiting β increases with the current until the q profile becomes flat over most of the plasma and $q \approx 2$ at the plasma edge. When this β value is exceeded the external kink takes the form of a rapidly growing mode with a large $m=2$ component. As shown by Rosenbluth, Monticello, Strauss, and White (1976), in a low-shear plasma the external kink can lead to large vacuum bubble formation and severe deformation of the equilibrium surfaces. In the nonlinear phase in a resistive plasma the effects of this mode would undoubtedly be very similar to the development of a large $m=2$ magnetic island, and hence would lead to disruption.

This possible role of the external kink in a tokamak disruption has been examined by Zakharov (1981). The success of the Troyon result makes it very plausible that kinks play a role in high-β disruptions. Simulation of the formation of vacuum bubbles in low-shear resistive plasmas has been carried out by Kurita *et al.* (1985).

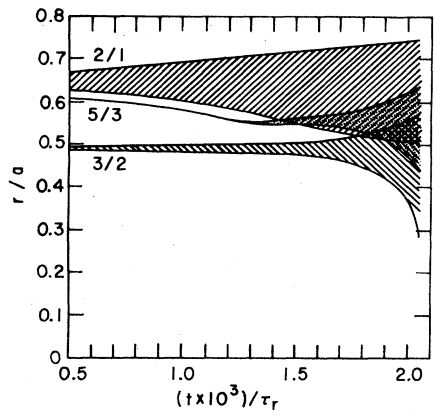

FIG. 16. The nonlinear evolution of magnetic islands, showing interaction of the 2/1, the 3/2, and the 5/3 state when overlap occurs.

E. Nonlinear cylindrical modes, $m=1$

If the toroidal current in a tokamak is made sufficiently large that the safety factor is less than one on axis, the x-ray emission typically shows a characteristic sawtooth behavior. At the plasma center, the x-ray intensity rises in a time consistent with ohmic heating, and then suddenly drops. Outside the $q=1$ surface the sawtooth is reversed, i.e., the x-ray intensity rises abruptly and decays slowly (Sauthoff, Goeler, and Stodiek 1978).

As originally conjectured by Kadomtsev (1975) and Monticello (1975), the $m=1$ mode is capable of evolving nonlinearly through a sequence of states, which ends with helical flux surfaces forming concentric cylinders, just as in the original state, but which results in a flattening of the current profile inside the $q=1$ surface and releases a corresponding amount of magnetic energy. Since the final state of this process can again acquire a central current peak through ohmic heating and the ensuing decrease in resistivity, the process can in principle be cyclic. The reconnection sequence proposed is shown in Fig. 17. The first sketch shows the initial helical flux contours with the $q=1$ surface shown as a dotted line. An initial $m=1$ perturbation causes the displacement of the central region, reconnection taking place at the x point. The two surfaces labeled 1 connect to form one surface, which withdraws from the x point [Fig. 17(b)]. The subsequent evolution of the area inside surface 1 does not involve the resistivity, so this area is conserved, as is the value of ψ, since $(d\psi/dt)=0$ neglecting resistivity. The same process occurs with the surfaces labeled 2,3 [Figs. 17(d) and 17(e)] until finally the initial 0 point (labeled 4) has been expelled through the x point and the flux contours have again returned to an axisymmetric equilibrium state. The resulting changes in the helical flux profile, the q profile, and the current profile are shown in Fig. 18. The flux

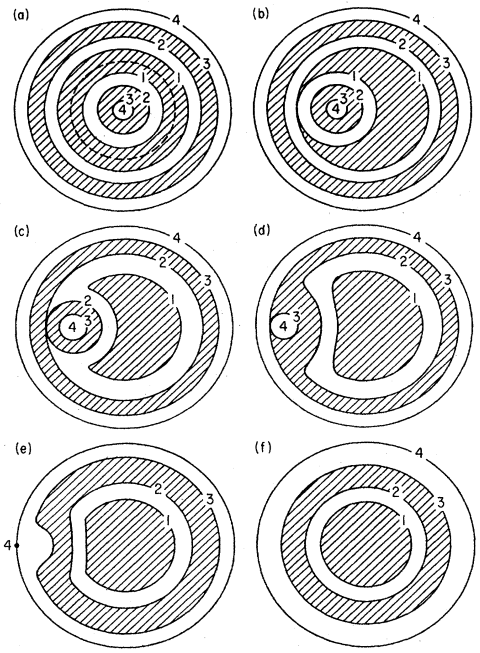

FIG. 17. The sequence of magnetic flux contours during the nonlinear evolution of the $m=1$ mode.

surface labeling in Fig. 18(a) corresponds to that in Fig. 17. The new ψ profile is easily obtained by recalling that ψ is conserved following the field in this process and that surfaces joining in the reconnection process have initially the same value of ψ. In the final state there is a discontinuity in $(d\psi/dr)$ at r_4. The safety factor profile (Fig. 18) is readily obtained by noting that

$$q(r)=[1+(R/r)(d\psi/dr)]^{-1}\ .$$

In the final state $q(0)=1$ and $q(r)$ is appreciably flattened out to r_4, where it is discontinuous. The current profile [Fig. 18(c)] is quite flat out to r_4, where it possesses a reverse current sheet. All three profiles are unchanged for $r>r_4$. The final state has much lower energy than the initial state, as is readily verified, but it is not clear from this analysis whether this final state is accessible nor at what rate it would proceed during its highly nonlinear evolution.

The nonlinear two-dimensional codes described in Sec. VI were used to investigate the process in detail and showed (Sykes and Wesson, 1976; Waddell, Rosenbluth, Monticello, and White, 1976; Danilov, Dnestrovskii, Kostomarov, and Popin, 1976; Dnestrovskii, Lysenko, and Smith, 1977) that this process was, in fact, nonlinearly possible as well as energetically favorable. The experimental time scale for the rapid phase of the sawtooth was consistent with the nonlinear behavior of the mode in many cases, but some experiments indicated a much more rapid phenomenon. The sequence of helical flux surfaces for the process obtained from a numerical code is shown in Fig. 19. The numerical simulations show that the mode continues growing at essentially its linear growth rate for almost the entire nonlinear process. The mode has a linear growth rate substantially larger than that of the $m=2$ mode, because it is ideally neutral stable (Sec. III). The invalidity of the constant ψ approximation makes the Rutherford analysis invalid. Numerical simu-

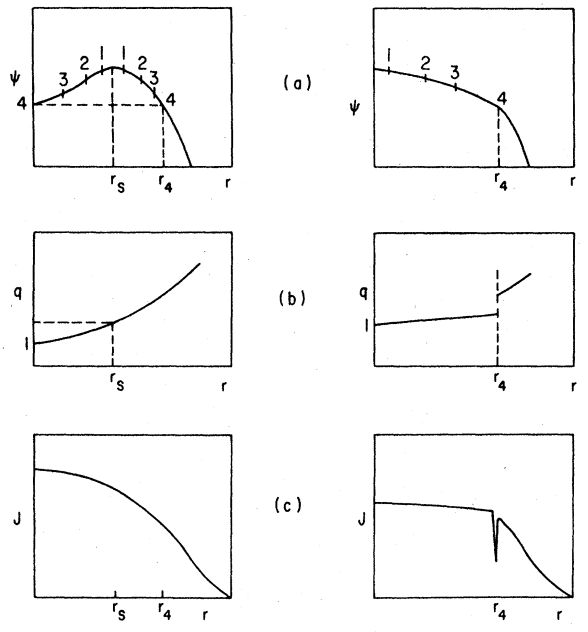

FIG. 18. The helical flux (a), safety factor profile (b), and current profile (c) before and after the $m=1$ evolution.

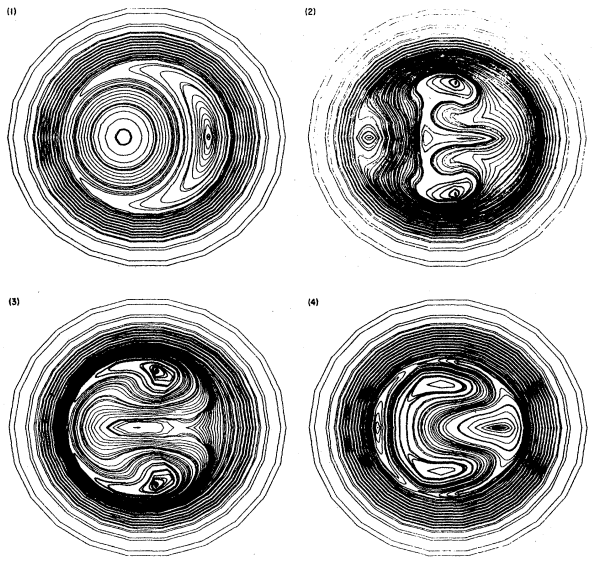

FIG. 19. Helical flux contours in the poloidal plane at selected times (normalized to the resistive time). The radius of the outermost contour is $r=0.4c$, and the singular surface is at $r=0.2a$. The peaked profile was used. Although the final stage looks very convoluted, the current profile is quite flat at this point. Inclusion of thermal conductivity allows this state to relax quickly to a configuration of concentric circles.

lations show that the current sheet at the x point scales even in the nonlinear development as $S^{2/3}$, so as to allow the entire transition to proceed on the time scale of the linear growth rate, but the narrow width of the current sheet makes numerical examination of the full evolution of the mode for very large values of S difficult. For most of the evolution no deviation from the linear growth rate is observed. Biskamp (1981) has shown that for very large S the island width also grows linearly in time when $w > r_s$. In this domain the kinetic energy of the mode has reached its maximum. The time for the subsequent completion of the evolution scales as $\eta^{-1/2}$, i.e., the reconnection proceeds at the Sweet-Parker rather than the Petschek rate, as discussed in Sec. III.

The very rapid evolution observed in some discharges remains a mystery and has been addressed by several authors. An ideal MHD analysis (Bussac, Pellat, Soule, and Tagger, 1984) indicates that a large island state is unstable to a vertically asymmetric displacement, perhaps resulting in a more rapid and violent final stage than is predicted by simulations that assume up-down symmetry. Dubois and Samain (1979a,1979b) have attempted to explain the very rapid evolution observed in some discharges by the development of turbulence associated with the island separatrix. Inclusion of finite Larmor radius effects can modify the nonlinear behavior. Biskamp (1981) finds that a diamagnetic frequency larger than the growth rate can even produce saturation. Lichtenberg (1984) has examined the development of large-scale stochasticity surrounding the island in the last stages of the island development. The stochasticity is generated by the nonlinear interaction of the mode with the $m=1, n=0$ field variation present in a toroidal equilibrium. Thus this is a phenomenon not observable with cylindrical code simulations. He finds that the stochastic mechanism predominates for cases with high shear, with $q<0.8$ on axis. The stochastic development modifies the time scale for the final stage of the disruption.

Further analysis of the complete sawtooth period, including the ohmic heating phase, and in particular the scaling of this period on various plasma parameters, has been attempted (Callen and Jahns, 1977; Jahns *et al.*, 1978; Waddell *et al.*, 1978; McGuire and Robinson, 1979). No treatment adequately explains all experiments.

F. Multiple tearing modes

In the initial or skin phase of a tokamak discharge, the current profile often assumes a hollow form, and the safety factor can have the same rational value of two values of the minor radius. This leads to the possibility of a pair of magnetic islands with the same helicity developing in a sequence of flux contours such as that shown in Fig. 20 for $m=2$. This is of interest because the mixing of the two islands produces a complicated flux topology, which should strongly affect radial heat and particle transport (Stix, 1973,1976). Redistribution of the plasma current along the convoluted lines would appear as fast radial

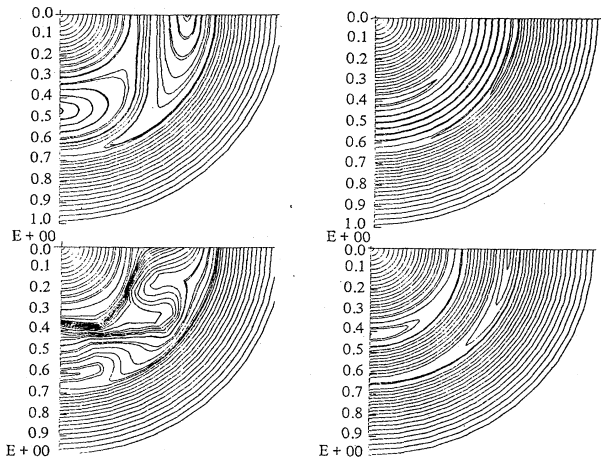

FIG. 20. The evolution of a pair of coupled magnetic islands of the same helicity. For this value of $S(10^4)$ no Rutherford regime is observed.

current penetration. Numerical simulation of this process was carried out by several authors (White, Monticello, Rosenbluth, and Waddell, 1977b; Carreras, Hicks, and Waddell, 1979; Schnack and Killeen, 1979).

The constant ψ approximation is not applicable for these modes for typical plasma parameters, since during the skin phase of the discharge the tearing layer is quite wide. For values of S of 10^4 the islands are observed to continue exponential growth over most of their history. In the linear regime, Pritchett, Lee, and Drake (1980) have shown that $\gamma\tau_A \sim S^{-1/3}$, provided the separation δ of the two singular surfaces is small, $\delta < (ka)^{7/9} S^{-1/9}$. For larger δ, $\gamma\tau_A$ scales as $S^{-3/5}$ as usual. The merging of the two modes as shown in Fig. 20 is not a necessary conclusion of their development, and Carreras, Hicks, and Waddell (1979) found a simple condition which the equilibrium must satisfy for the islands to merge before they separately saturate through the same mechanism leading to saturation of the $m=2$ mode in a monotonically decreasing current profile. If S is sufficiently large, the islands are observed to enter a Rutherford regime.

Detailed comparison of the process with the observed anomalous current penetration in tokamak discharges has been done by Hawryluk *et al.* (1980), and Meyerhofer *et al.* (1984).

G. Reversed-field pinch

The reversed-field pinch configuration is produced by a toroidal current caused to flow in a toroidal field. This current is responsible for plasma compression and confinement. After an initial highly turbulent phase the plasma settles into a more quiescent state, which is essentially the same for all discharges. This state is approximately given by $\mathbf{J}=\mu\mathbf{B}$ (Taylor, 1974). The magnetic field exhibits a dynamo effect with field reversal occurring near the plasma edge. Simulations of the field reversal have been

carried out by Strauss (1984). The discharge is thus characterized by a q profile with a value on axis which is small [$q(0) \sim \frac{1}{10}$], monotonically decreasing with minor radius to become slightly negative at the plasma edge. Thus the relevant rational surfaces are given by $m = 1,2$ and n large. The nonlinear behavior of these modes is found to be significantly different from that observed in a tokamak configuration (Caramara, Nebel, and Schnack, 1983; Holmes *et al.*, 1984). There are typically several unstable modes in the initial configuration having singular surfaces within the field reversal surface. Because of the relatively large resistivity and the close proximity of these modes, nonlinear behavior becomes important earlier than in a tokomak discharge, and the spontaneous fluctuations of the magnetic field in the steady state are much larger than in a tokamak (Antoni and Ortolani, 1983). A double reconnection process is observed when the dynamics leads to sufficient β and when the singular surface is close to the center of the plasma. The nonlinear coupling of different helicities, in contrast to the tokamak case, is found to be stabilizing. The role of this stabilization in the formation of dynamo states has yet to be investigated.

ACKNOWLEDGMENTS

This review is a revised and updated version of my Handbook of Plasma Physics article (White, 1983). I am grateful for useful discussions with many scientists working toward the promise of controlled thermonuclear fusion, in particular D. A. Monticello, M. S. Chance, W. Park, J. A. Greene, F. W. Perkins, A. H. Boozer, P. H. Rutherford, and A. H. Reiman.

REFERENCES

Adler, A. E., R. M. Kulsrud, and R. B. White, 1980, Phys. Fluids **23**, 1375.
Antoni, V., and S. Ortolani, 1983, Plasma Phys. **25**, 799.
Arnol'd, V. I., 1963, Russ. Math. Sur. **18**, 9.
Arsenin, V. V., L. I. Arkmenkov, N. V. Ivanov, and A. M. Kakurin, 1978, Princeton Plasma Phys. Lab. Translation PPPL-126.
Arsenin, V. V., and A. V. Chuyanov, 1977, Usp. Fiz. Nauk. **123**, 83.
Asumi, M., 1985, private communication.
Bateman, G., and R. Morris, 1985, Phys. Fluids (to be published).
Bernstein, I. B., E. A. Frieman, M. D. Kruskal, and R. M. Kulsrud, 1958, Proc. R. Soc. London, Ser. A **244**, 17.
Biskamp, D., 1978, Nucl. Fusion **18**, 1059.
Biskamp, D., 1981, Phys. Rev. Lett. **46**, 1522.
Biskamp D., 1985, in *Workshop on Magnetic Reconnection and Turbulence, Cargese,* edited by D. Gresillon (Ecole Polytechnique, Paris, to be published).
Biskamp, D., and H. Welter, 1978, Bull. Am. Phys. Soc. **23**, 872.
Bondeson, A., 1983, Phys. Rev. Lett. **51**, 1668.
Bondeson, A., and J. R. Sobel, 1984, Phys. Fluids **27**, 2028.
Boozer, A. H., 1983, Phys. Fluids **26**, 1288.
Boozer, A. H., and R. B. White, 1982, Phys. Rev. Lett. **49**, 786.
Brushlinskii, K. V., A. M. Zaborov, and S. L. Syrovatskii, 1980, Sov. J. Plasma Phys. **6**, 165.
Bussac, M. N., R. Pellat, J. L. Soule, and M. Tagger, 1984, Phys. Lett. **105**, 51.
Bussac, M. N., D. Edery, R. Pellat, and J. L. Soule, 1977, in *Plasma Physics and Controlled Nuclear Fusion Research 1976: Proceedings of the 6th International Conference, Berchtesgaden* (IAEA, Vienna), Vol. I, p. 607.
Bussac, M. N., R. Pellat, D. Edery, and J. Soule, 1977, Phys. Rev. Lett. **35**, 1638.
Callen, J. D., B. V. Waddell, B. Carreras, M. Azumi, P. J. Catto, H. R. Hicks, J. A. Holmes, D. K. Lee, S. J. Lynch, J. Smith, M. Soler, K. T. Tsang, and J. C. Whitson, 1979, in *Plasma Physics and Controlled Nuclear Fusion Research 1978: Proceedings of the 7th International Conference . . . Innsbruck* (IAEA, Vienna), Vol. 1, p. 415.
Callen, J. D., and G. L. Jahns, 1977, Phys. Rev. Lett. **38**, 491.
Caramara, E. J., R. A. Nebel, and D. D. Schnack, 1983, Phys. Fluids **26**, 1305.
Carrreras, B., H. R. Hicks, J. A. Holmes, and B. V. Waddell, 1980, Phys. Fluids **23**, 811.
Carreras B., H. R. Hicks, and B. V. Waddell, 1979, Nucl. Fusion **19**, 583.
Chu, M. S., and J. K. Lee, 1983, Phys. Fluids **26**, 766.
Coppi, B., R. Galvao, R. Pellat, M. N. Rosenbluth, and P. H. Rutherford, 1976, Fiz. Plazmy **2**, 961 [Sov. J. Plasma Phys. **2**, 533 (1976)].
Cowley S., R. Kulsrud, and T. H. Hahm, 1985, Phys. Fluids (to be published).
Danilov, A. F., Yu. N. Dnsetrovskii, D. P. Kostomarov, and A. M. Popin, 1976, Fiz. Plazmy **2**, 167 [Sov. J. Plasma Phys. **2**, 93 (1976)].
Diamond, P. H., R. D. Hazeltine, Z. G. An, B. A. Carreras, and H. R. Hicks, 1984, Phys. Fluids **27**, 1449.
Dnestrovskii, Yu. N., S. E. Lysenko, G. V. Pereversev, K. N. Tarasyan, and D. P. Kostomarov, 1979, in *Plasma Physics and Controlled Nuclear Fusion Research 1978: Proceedings of the 7th International Conference . . . Innsbruck* (IAEA, Vienna), Vol. 1, p. 443.
Dnestroskii, Yu. N., D. P. Kostomarov, V. G. Pereverzev, and K. N. Tarasyan, 1978, Fiz. Plazmy **4**, 1001 [Sov. J. Plasma Phys. **4**, 557 (1978)].
Dnestrovskii, Yu. N., S. E. Lysenko, and R. Smith, 1977, Sov. J. Plasma Phys. **3**, 9.
Drake, J. F., and Y. C. Lee, 1977, Phys. Rev. Lett. **39**, 453.
Dubois, M., and A. Samain, 1979a, Nucl. Fusion **20**, 1101.
Dubois, M., and A. Samain, 1979b, Plasma Phys. **21**, 101.
Finn, J. M., 1975, Nucl. Fusion **15**, 845.
Finn, J. M., 1977, Phys. Fluids **20**, 1749.
Furth, H. P., 1963, in *Propagation and Instabilities in Plasmas,* edited by W. T. Futterman (Stanford University, Stanford, CA), p. 87.
Furth, H. P., J. Killeen, and M. N. Rosenbluth, 1963, Phys. Fluids **6**, 459.
Furth, H. P., P. H. Rutherford, and H. Selberg, 1973, Phys. Fluids **16**, 1054.
Glasser, A. H., H. P. Furth, and P. H. Rutherford, 1977, Phys. Rev. Lett. **38**, 234.
Glasser, A. H., J. M. Greene, and J. L. Johnson, 1976, Phys. Fluids **19**, 567.
Grad, H., P. N. Hu, and D. C. Stevens, 1975, Proc. Natl. Acad.

Sci. U.S.A. **72**, 3789.
Grad, H., and H. Rubin, 1958, in *United Nations Peaceful Uses of Atomic Energy,* edited by John H. Martens *et al.* (United Nations, Geneva, 1958), Vol. 31, p. 190.
Hameiri, E., 1979, J. Plasma Phys. **22**, 245.
Hawryluk, R. J., N. Bretz, D. Dimock, E. Hinnov, D. Johnson, D. A. Monticello, D. McClune, and S. Suckewer, 1980, Princeton Plasma Phys. Lab. Report No. PPPL-1572.
Holmes, A. J., B. A. Carreras, T. C. Hendor, H. R. Hicks, V. E. Lynch, Z. G. An, and P. H. Diamond, 1984, Oak Ridge National Laboratory Report Number ORNL TM-9148.
Ivanov, N. V., 1983, Sov. J. Plasma Phys. **9**, 407.
Ivanov, N. V., A. M. Kakurin, and A. N. Chudnovskii, 1984, Sov. J. Plasma Phys. **10**, 38.
Izzo, R., D. A. Monticello, J. DeLucia, W. Park, and C. M. Ryu, 1985, Phys. Fluids **28**, 903.
Jahns, G. L., M. Soler, B. V. Waddell, J. D. Callen, and H. R. Hicks, 1978, Nucl. Fusion **18**, 609.
Kadomtsev, B. B., 1975, Fiz. Plazmy **1**, 710 [Sov. J. Plasma Phys. **1**, 389 (1975)].
Karger, F., *et al.*, 1979, in *Proceedings of the IAEA Symposium on Current Disruptions in Toroidal Devices,* edited by K. Lackner and H. P. Zehrfield (Max Planck-Institut für Plasmaphysik, Garching).
Karger, F., K. Lockner, G. Fussman, B. Cannici, W. Engelhardt, J. Gernhardt, D. Glock, D. E. Groening, O. Kluber, G. Lisitano, H. M. Mayer, D. Meisel, P. Morandi, S. Sesnic, F. Wagner, and H. P. Zehrfeld, 1977, in *Plasma Physics and Controlled Fusion Research 1976: Proceedings of the 6th International Conference ... Berchtesgaden* (IAEA, Vienna), Vol. I, p. 267.
Kleva, R. G., J. F. Drake, and A. Bondeson, 1984, Phys. Fluids **27**, 769.
Kolmogorov, A. N., 1957, in *Proceedings of the International Congress of Mathematicians, Amsterdam* (North-Holland, Amsterdam), Vol. 1, p. 715.
Kotschenreuther, M., R. D. Hazeltine, and P. J. Morrison, 1985, Phys. Fluids **28**, 294
Kurita, G., M. Azumi, T. Tsunematsu, and T. Takeda, 1983, Plasma Phys. **25**, 1097.
Kurita, G., M. Azumi, T. Tuda, and T. Tsunematsu, T. Takizuka, Y. Tanaka, and T. Takeda, 1985, Plasma Phys. Controlled Nucl. Fusion **27**, 579.
Lichtenberg, A. J., 1984, Nucl. Fusion **24**, 1277.
Johnson, D., D. C. McCune, and K. McGuire, 1984, Nucl. Fusion **24**, 1303.
McGuire, K., and D. C. Robinson, 1979, in *Proceedings of the IAEA Symposium on Current Disruptions in Toroidal Devices,* edited by K. Lackner and H. P. Zehrfield (Max Planck-Institut für Plasmaphysik, Garching).
Meyerhofer, D. D., R. J. Goldston, R. Kaita, A. Cavallo, B. Grek, D. Johnson, D. C. McCane, K. McGuire, and R. B. White, 1985, Nucl. Fusion **25**, 321.
Mirnov, S. V., and I. B. Semenov, 1971, Sov. Phys. JETP **33**, 1134.
Monticello, D. A., 1975, private communication.
Monticello, D. A., and R. B. White, 1980, Phys. Fluids **23**, 366.
Monticello, D. A., R. B. White, and M. N. Rosenbluth, 1979, in *Plasma Physics and Controlled Nuclear Fusion Research 1978: Proceedings of the 7th International Conference, Innsbruck* (IAEA, Vienna), Vol. 1, p. 605.
Monticello, D. A., W. Park, S. C. Jardin, M. S. Chance, R. L. Dewar, R. B. White, R. C. Grimm, J. Manickam, H. R. Strauss, J. L. Johnson, J. M. Greene, A. H. Glasser, P. K. Kaw, P. H. Rutherford, and E. J. Valeo, 1981, in *Plasma Physics and Controlled Nuclear Fusion Research 1980: Proceedings of the 8th International Conference, Brussels* (IAEA, Vienna), Vol. I, p. 227.
Morozov, A. I., and L. S. Solov'ev, 1963, in *Voprosy Teorii Plazmy* (Atomizdat, Moscow); English translation published 1966 as *Reviews of Plasma Physics* (Consultants Bureau, New York), Vol. II, p. 1.
Moser, J., 1962, Nachr. Akad. Wiss. Göttingen No. 1, p. 1.
Newcomb, W. A., 1958, Ann. Phys. **3**, 347.
Park, W., D. A. Monticello, R. B. White, and S. C. Jardin, 1980, Nucl. Fusion **20**, 1181.
Park, W., D. A. Monticello, and R. B. White, 1984, Phys. Fluids **27**, 137.
Parker, E. N., 1963, Astrophys. J. Suppl. **77**, 8:177.
Petschek, H. E., 1964, in *AAS-NASA Symposium on the Physics of Solar Flares,* edited by W. N. Hess (NASA, Washington, D.C.), NASA SP-50, p. 425.
Pogutse, O. P., and E. I. Yurchenko, 1977, Sov. J. Plasma Phys. **3**, 283.
Poincaré, H., 1892—1899, *Les Nouvelles Méthodes de la Mécanique Céleste* (English translation published 1967, NASA, Washington, D.C.).
Pollard, R., M. Turner, A. Sykes, and J. A. Wesson, 1979, in *Proceedings of the IAEA Symposium on Current Disruptions in Toroidal Devices,* edited by K. Lackner and H. P. Zehrfield (Max Planck-Institute für Plasmaphysik, Garching).
Pritchett, P. L., Y. C. Lee, and J. F. Drake, 1980, Phys. Fluids **23**, 1368.
Priest, E. R., 1983, Plasma Phys. **25**, 161.
Reiman, A. H., 1983, Phys. Fluids **26**, 1338.
Rosenbluth, M. N., D. A. Monticello, H. R. Strauss, and R. B. White, 1976, Phys. Fluids **19**, 1987.
Rutherford, P. H., 1973, Phys. Fluids **16**, 1903.
Rutherford, P. H., and H. P. Furth, 1971, Princeton Plasma Phys. Lab. Report No. Matt-872.
Sato, T., and T. Hayashi, 1979, Phys. Fluids **22**, 1189.
Sauthoff, N. R., S. V. Goeler, and W. Stodiek, 1978, Nucl. Fusion **18**, 1445.
Schnack, D., and J. Killeen, 1979, Nucl. Fusion **19**, 877.
Scott, B. D., A. B. Hassam, and J. F. Drake, 1985, Phys. Fluids **28**, 275.
Shafranov, V. D., 1966, Rev. Plasma Phys. **2**, 103.
Shafranov, V. D., 1970, Zh. Tekh. Fiz. **40**, 240 [Sov. Phys. Tech. Phys. **15**, 175 (1970)].
Sonnerip, B. U. O., 1979, in *Solar System Plasma Physics,* edited by E. N. Parker, C. F. Kennel, and L. J. Lanzerotti (North-Holland, Amsterdam), Vol. III, p. 45.
Stenzel, R. L., W. Gekelman, and N. Wild, 1982, J. Geophys. Res. **87**, 111.
Stix, T., 1973, Phys. Rev. Lett. **30**, 833.
Stix, T., 1976, Phys. Rev. Lett. **36**, 521.
Strauss, H. R., 1976, Phys. Fluids **19**, 134.
Strauss, H. R., 1977, Phys. Fluids **20**, 1354.
Strauss, H. R., 1984, Phys. Fluids **27**, 2580.
Strauss, H. R., W. Park, D. A. Monticello, R. B. White, S. C. Jardin, M. S. Chance, A. M. M. Todd, and A. H. Glasser, 1980, Nucl. Fusion **20**, 638.
Sweet, P. A., 1958, in *Electromagnetic Phenomena in Cosmical Physics,* IAU Symposium No. 6, edited by B. Lehnert (Cambridge University, Cambridge), p. 123.
Sykes, A., and J. A. Wesson, 1976, Phys. Rev. Lett. **37**, 140.
Skyes, A., and J. A. Wesson, 1980, Phys. Rev. Lett. **44**, 1215.
Taylor, J. B., 1974, Phys. Rev. Lett. **33**, 1139.

Troyon, F., R. Gruber, H. Saurenmann, S. Semenzato, and S. Succi, 1984, Plasma Phys. Controlled Fusion **26**, 209.
Ugai, M., and T. Tsuda, 1977, J. Plasma Phys. **17**, 337.
Vasyliunas, V. M., 1975, Rev. Geophys. Space Phys. **13**, 303.
Waddell, B. V., B. Carreras, H. R. Hicks, and J. A. Holmes, 1979, Phys. Fluids **22**, 896.
Waddell, B. V., G. L. Jahns, J. D. Callen, and H. R. Hicks, 1978, Nucl. Fusion **18**, 735.
Waddell, B. V., M. N. Rosenbluth, D. A. Monticello, and R. B. White, 1976, Nucl. Fusion **16**, 528.
Waddell, B. V., M. N. Rosenbluth, D. A. Monticello, and R. B. White, and B. Carreras, 1978, in *Theoretical and Computational Plasma Physics: Selected Lectures Presented at Two Meetings . . . Trieste* (IAEA, Vienna), p. 79.
Welter, H., and D. Biskamp, 1978, Bull. Am. Phys. Soc. **23**, 872.
Wesson, J. A., 1966, Nucl. Fusion **6**, 130.
Wesson, J. A., 1978, Nucl. Fusion **18**, 87.
Wesson, J. A., and M. F. Turner 1982, Nucl. Fusion **22**, 1069.
White, R. B., 1983, in *Handbook of Plasma Physics,* edited by M. N. Rosenbluth and R. Z. Sagdeev (North-Holland, Amsterdam), Vol. 1, Chap 3.5.
White, R. B., 1984, in *Statistical Physics and Chaos in Fusion Plasmas,* edited by C. W. Horton, Jr. and L. E. Reichl (Wiley, New York), p. 209.
White, R. B., and D. A. Monticello, 1980, Princeton Plasma Phys. Laboratory Report, 1974.
White, R. B., D. A. Monticello, and M. B. Rosenbluth, 1977, Phys. Rev. Lett. **39**, 1618.
White, R. B., D. A. Monticello, M. N. Rosenbluth, and B. V. Waddell, 1977a, Phys. Fluids **20**, 800.
White, R. B., D. A. Monticello, M. N. Rosenbluth, and B. V. Waddell, 1977b, in *Plasma Physics and Controlled Nuclear Fusion Research 1976: Proceedings of the 6th International Conference . . . Berchtesgaden* (IAEA, Vienna), Vol. I, p. 569.
White, R. B., W. Park, D. A. Monticello, and H. R. Strauss, 1979, in *Proceedings of the Symposium on Current Disruption in Toroidal Devices,* edited by K. Lackner and H. P. Zehrfield (Max Planck-Institut für Plasmaphysik, Garching).
Yoshioka, Y., S. Kinoshita, and T. Kobayashi, 1984, Nucl. Fusion **24**, 565.
Zakharov, L. E., 1981, Sov. J. Plasma Phys. **7**, 8.